Article

TRANSPARENT PROCESS

EMBO reports

Myotubularin functions through actomyosin to interact with the Hippo pathway

Liang Hu[1], Wyatt Brichalli[2], Naren Li[1], Shifan Chen[3], Yaqing Cheng[1], Qinfang Liu[3], Yulan Xiong[3,*] & Jianzhong Yu[1,**]

Abstract

The Hippo pathway is an evolutionarily conserved developmental pathway that controls organ size by integrating diverse regulatory inputs, including actomyosin-mediated cytoskeletal tension. Despite established connections between the actomyosin cytoskeleton and the Hippo pathway, the upstream regulation of actomyosin in the Hippo pathway is less defined. Here, we identify the phosphoinositide-3-phosphatase Myotubularin (Mtm) as a novel upstream regulator of actomyosin that functions synergistically with the Hippo pathway during growth control. Mechanistically, Mtm regulates membrane phospholipid PI(3)P dynamics, which, in turn, modulates actomyosin activity through Rab11-mediated vesicular trafficking. We reveal PI(3)P dynamics as a novel mode of upstream regulation of actomyosin and establish Rab11-mediated vesicular trafficking as a functional link between membrane lipid dynamics and actomyosin activation in the context of growth control. Our study also shows that MTMR2, the human counterpart of *Drosophila* Mtm, has conserved functions in regulating actomyosin activity and tissue growth, providing new insights into the molecular basis of MTMR2-related peripheral nerve myelination and human disorders.

Keywords Actomyosin; Hippo pathway; Myotubularin; PI(3)P; Rab11

Subject Categories Cell Adhesion, Polarity & Cytoskeleton; Development; Signal Transduction

DOI 10.15252/embr.202255851 | Received 25 July 2022 | Revised 1 October 2022 | Accepted 7 October 2022 | Published online 26 October 2022

EMBO Reports (2022) 23: e55851

Introduction

The Hippo pathway is an evolutionarily conserved pathway that controls organ size and tissue homeostasis during animal development (Yu *et al*, 2015; Zheng & Pan, 2019). Dysregulated Hippo pathway has been implicated in a wide range of human disorders, including cancers (Calses *et al*, 2019; Han, 2019; Ma *et al*, 2019; Zheng & Pan, 2019). The core of the Hippo pathway is a kinase cascade comprised of the Ste20 family kinase Hippo (Hpo) and the NDR family kinase Warts (Wts), and their regulatory proteins Salvador (Sav) and Mats, respectively. Downstream of the kinase cascade is the transcriptional machinery, including the transcriptional co-activator Yorkie (Yki) and the TEAD/TEF family transcription factor Scalloped (Sd) (Tapon & Harvey, 2012; Meng *et al*, 2016). In *Drosophila*, inactivation of the kinase cascade or hyperactivation of Yki/Sd leads to massive tissue overgrowth, a combined result of excessive cell proliferation and diminished apoptosis (Pan, 2007). Upstream of the kinase cascade are several proteins identified as upstream regulators, including Merlin (Mer), Expanded (Ex), Fat (ft), and Kibra (Yu & Guan, 2013; Meng *et al*, 2016; Choi, 2018; Fulford *et al*, 2018). Loss-of-function of these upstream regulators results in relatively mild tissue overgrowth compared to those of the core components (Grusche *et al*, 2010). These phenotypic differences indicate that the Hippo pathway coordinates divergent signal inputs and stimuli via distinct and yet to be fully understood mechanisms.

Recent studies have recognized the apical cytocortex of epithelial cells as a critical site for Hippo pathway activation and regulation (Yu & Guan, 2013; Rausch & Hansen, 2020). Indeed, cell polarity proteins like Crumbs (Crb) and Lethal giant larvae (Lgl) are known Hippo pathway regulators (Grzeschik *et al*, 2010; Ling *et al*, 2010). Furthermore, the Hippo pathway upstream regulators Mer, Ex, and Kibra are apical membrane-associated (Maitra *et al*, 2006; Yu *et al*, 2010; Su *et al*, 2017). The core kinase Wts is recruited to the plasma membrane for activation via direct binding with Mer (Yin *et al*, 2013). In addition, disruption of the Hippo pathway leads to the accumulation of apical proteins and expansion of the apical domain (Genevet *et al*, 2009; Hamaratoglu *et al*, 2009). More recently, a non-transcriptional function of Yki at the cell cortex has been revealed (Xu *et al*, 2018), further suggesting the complexity of the Hippo pathway regulation at the apical cytocortex.

The actomyosin network mediates cytoskeletal tension underneath the plasma membrane. Studies from both fly and mammalian cell cultures have implicated that actomyosin-mediated cytoskeletal tension plays an important role in regulating the Hippo pathway (Zhao *et al*, 2012; Sun & Irvine, 2016). In *Drosophila*, modulating F-actin organization leads to dysregulated Hippo signaling activity and growth defects, possibly through

1 Department of Physiology and Neurobiology, University of Connecticut, Storrs, CT, USA
2 Department of Anatomy & Physiology, Kansas State University College of Veterinary Medicine, Manhattan, KS, USA
3 Department of Neuroscience, University of Connecticut School of Medicine, Farmington, CT, USA
*Corresponding author. Tel: +1 8606794116; E-mail: yxiong@uchc.edu
**Corresponding author. Tel: +1 8604865440; E-mail: jianzhong.yu@uconn.edu

sensing mechanical forces (Fernandez *et al*, 2011; Sansores-Garcia *et al*, 2011; Matsui & Lai, 2013; Seo & Kim, 2018). A study on *Drosophila* wing growth identified Ajuba and Warts protein complex as a molecular link between cytoskeletal tension and Hippo signaling activation (Rauskolb *et al*, 2014). Further studies characterized spectrin-based membrane skeleton as an upstream regulator of the Hippo pathway by modulating actomyosin activity (Deng *et al*, 2015, 2020). In mammalian cells, mechanical signals induced by cytoskeleton reorganization have been reported as crucial regulatory inputs of the Hippo pathway transcriptional coactivators YAP/TAZ (Dupont *et al*, 2011; Aragona *et al*, 2013; Meng *et al*, 2016). Despite these advances, little is known about the upstream regulators of actomyosin in the context of growth control and their regulatory relationships with the Hippo pathway. In addition, the molecular mechanism underlying the interplays among apical cytocortex organization, actomyosin activity, and Hippo signaling remains to be elucidated.

In this study, we report the identification of lipid phosphatase Myotubularin (Mtm) as a novel upstream regulator of actomyosin that functions synergistically with the Hippo pathway in growth control. Mtm is a member of the myotubularin family of phosphatidylinositol-3-phosphatases with known function in controlling PI(3)P dynamics (Velichkova *et al*, 2010). Our study suggests that Mtm regulates actomyosin activity through PI(3)P dynamics and Rab11-mediated vesical trafficking. We further show that Myotubularin Related Protein 2 (MTMR2), the human homolog of *Drosophila mtm*, has conserved function in regulating actomyosin activity and tissue growth. Our study, therefore, provides membrane phospholipid PI(3)P dynamics as a novel upstream regulation of actomyosin in the context of growth control.

Results

Identification of Mtm as a novel growth regulator

In an ethyl methanesulfonate (EMS)-induced mutagenesis screen for novel growth regulators using *eyeless* FLP/FRT technique in *Drosophila*, we identified a lethal mutation (*40-B89*) on chromosome 2 L that caused overgrowth of mosaic eyes (Fig 1A and B). Through complementation tests, we found that *40-B89* failed to complement two lethal deficiency lines: Df(2L)ED343 and Df(2L)BSC353. Further analysis identified 11 overlapping genes deleted in these two deficiency lines. DNA sequencing analysis revealed a missense mutation of the gene, *myotubularin* (*mtm*), that changed Gly^{447} of Mtm to Asp^{447} (Fig 1E; Appendix Fig S1A and B). We therefore renamed *40-B89* as mtm^{G447D}. To confirm that the observed overgrowth phenotype was caused by *mtm* mutation, we used CRISPR/Cas9 system to generate a novel null allele (mtm^{null}) containing a frameshift mutation, leading to the introduction of a stop codon at the 77^{th} amino acid threonine (Thr^{77}) (Fig 1E; Appendix Fig S1B and C). Both mtm^{null} and mtm^{G447D} alleles exhibited second instar larva lethality, and they failed to complement each other, suggesting the essential role of Mtm during *Drosophila* development. mtm^{null} produced a similar larger eye as mtm^{G447D}, confirming that *mtm* is responsible for the observed overgrowth phenotype (Fig 1C and D). Taken together, these results suggest that Mtm is a novel negative growth regulator.

Loss-of-*mtm* results in increased interommatidial cell numbers and hippo pathway target gene expression

During fly pupal retina development, a group of excessive cells is removed by apoptosis to ensure each ommatidium is surrounded by a single layer of pigment cells called interommatidial cells (Cagan & Ready, 1989; Wolff & Ready, 1991). An abnormal increase in interommatidial cells has been shown to be closely related to eye overgrowth (Hamaratoglu *et al*, 2006). We therefore asked whether Mtm regulates interommatidial cell number during eye development. Indeed, we found that *mtm* mutant clones contained an average of 5.3 extra interommatidial cells per ommatidial cluster (Fig 1F and G). Alteration of interommatidial cell number in pupal retina is a characteristic of defective Hippo signaling (Hamaratoglu *et al*, 2006). The increased eye size and the extra interommatidial cell number observed in *mtm* mutant flies suggest a potential relationship between Mtm and the Hippo pathway. To test this possibility, we first examined whether Mtm regulates the expression of *diap1* and *ex*, two well-known Hippo pathway target genes. Interestingly, *mtm* mutant clones in the eye imaginal disc showed increased Diap1 and Ex levels (Fig 1H and I), indicating that Mtm regulates Hippo pathway target gene expression. Next, we explored whether Mtm regulates the localization and phosphorylation of Yki, the transcriptional co-activator of the Hippo pathway. We found that loss-of-*mtm* promoted nucleus accumulation of Yki in wing discs (Fig 1J). Consistently, depletion of Mtm expression in Kc167 cells decreased the phosphorylation level of Yki (Fig 1K). Taken together, these results indicate that Mtm functions as a novel regulator of the Hippo pathway.

Figure 1. Identification of Mtm as a novel growth regulator.

A–D Images of a representative wild-type adult eye (A) or adult eyes containing *mtm* mutant clones (B and C). Quantification of relative eye sizes ($n = 10$) (D).

E Schematic diagram of *Drosophila* Mtm protein (top; Dm) and its human homolog MTMR2 (bottom; Hs). *mtm* mutant alleles from this study are indicated.

F, G A pupal eye disc containing *mtm* mutant clones (marked by the absence of GFP) was stained for Dlg. Note the increased interommatidial cells in the *mtm* mutant clone. Quantification of numbers of interommatidial cells per ommatidium ($n = 10$) (G). Scale bar = 10 μm.

H, I Third instar larval eye discs containing *mtm* mutant clones (marked by the absence of GFP) were stained for the Hippo pathway target genes *diap1* and *ex*. Note the increased expressions of Diap1 and Ex in *mtm* mutant clones indicated (arrows). Scale bars = 10 μm.

J A third instar larval wing disc containing *mtm* mutant clones (marked by the absence of GFP) was stained for Yki and DAPI. Note increased Yki nuclear localization in *mtm* mutant clone. Scale bar = 10 μm.

K RNAi of Mtm reduces Yki phosphorylation. Kc167 cells were incubated with dsRNA of *gfp* or *mtm* for 3 days before western blot analysis. Total cell lysates were probed with anti-phospho-Yki (p-Yki) antibody. Note that RNAi of *mtm* decreased Yki phosphorylation.

Data information: Data are shown as mean ± SEM, ***$P < 0.001$, ****$P < 0.0001$, Student's *t*-test. "*n*" indicates the numbers of samples used for the statistical analysis. D and G represent results from one of three biological replicates.

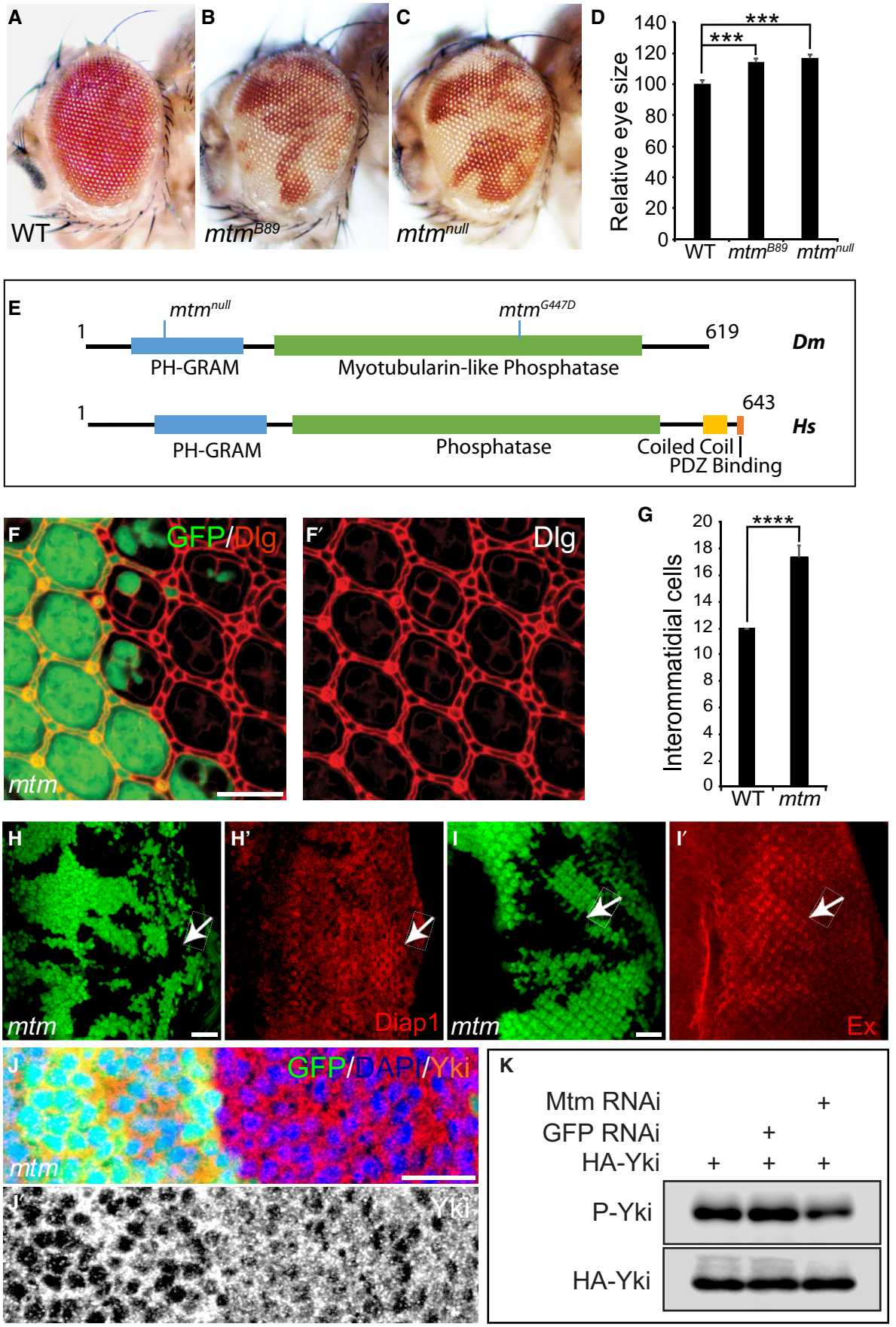

Figure 1.

Mtm functions synergistically with hippo pathway upstream regulators in growth control

To further test the regulatory relationships between Mtm and the Hippo pathway, we examined the genetic interactions between Mtm and Hippo pathway upstream regulators. The overgrowth of upstream regulators such as *mer*, *ex*, *ft*, or *kibra* single mutant is relatively mild (Fig 2A–E). Loss-of-*mtm* exhibited a similar mild eye overgrowth (Fig 2F). Strikingly, *mer; mtm* double mutant eye exhibited a much stronger overgrowth phenotype than the respective single mutants (Fig 2G). Moreover, while single mutants of *mer* and *mtm* resulted in a mild increase in interommatidial cell number (an average of 4.7 and 5.3 extra cells per cluster, respectively, Fig 2B′ and F′), *mer; mtm* double mutant flies showed a massive increase in interommatidial cells (an average of 25.1 extra cells per cluster, Fig 2G′). In addition to *mer; mtm*, both *ex*; *mtm* and *ft*; *mtm* double mutant eyes displayed a massive overgrowth phenotype (Fig 2H and I; Appendix Fig S2) and a much greater number of interommatidial cells (Fig 2H′ and I′). Similar overgrowth and extra interommatidial cells were also observed in *mtm*; *kibra* double mutant flies (Fig 2J and J′). Importantly, the massive overgrowth was also found in the adult nota of *ex*; *mtm* and *ft*; *mtm* double mutant flies (Fig 2K–P), suggesting Mtm functions as a general growth regulator in multiple tissues. Strong increases in Diap1 and Ex proteins were also found in *mer; mtm* double mutant clones (Fig 2Q and R), correlating with the relative severity of overgrowth phenotypes seen in these double mutant flies. Taken together, these results suggest that Mtm functions synergistically with Hippo pathway upstream regulators to control tissue growth.

Mtm growth suppression function requires both PH-GRAM domain and phosphatase domain

Next, we investigated how Mtm regulates tissue growth and interacts with the Hippo pathway at the molecular level. Mtm is a member of the myotubularin family of phosphatidylinositol-3-phosphatases containing two highly conserved functional domains, an N-terminal PH-GRAM domain and a C-terminal myotubularin-like phosphatase domain (Fig 3A). In humans, mutations identified in both domains of MTMR2, the human homolog of *Drosophila* Mtm, have been reported to be responsible for the development of the Charcot–Marie-Tooth-type 4B1 (CMT4B1) disease, a hereditary severe autosomal recessive motor and sensory neuropathies characterized by focally folded myelin of the peripheral nerves, indicating the importance of these two domains in CMT4B1 pathogenesis (Begley *et al*, 2003; Previtali *et al*, 2007). To further elucidate the growth suppression function of Mtm, we generated novel mutant flies carrying mutations within the functional domains of Mtm using the CRISPR/Cas9 technique (Fig 3A; Appendix Fig S1B). One mutant allele we obtained contains a deletion of four consecutive amino acids (*Δ*69–72) in the N-terminal PH-GRAM domain, which we named $mtm^{\Delta N}$. We also obtained a mutant allele carrying a deletion of four consecutive amino acids (*Δ*558–561) in the C-terminal myotubularin-like phosphatase domain, which we named $mtm^{\Delta C}$ (Fig 3A). Compared to the wild-type protein, $Mtm^{\Delta C}$ exhibited significantly decreased PI3P phosphatase activity, suggesting the four consecutive amino-acid deletion impairs its phosphatase activity (Appendix Fig S3I). Both $mtm^{\Delta N}$ and $mtm^{\Delta C}$ alleles are lethal and failed to complement each other and failed to complement mtm^{G447D} and mtm^{null} alleles, further suggesting the important physiological function of these two domains. Notably, both $mtm^{\Delta N}$ and $mtm^{\Delta C}$ alleles caused similar increased interommatidial cells comparable to the mtm^{null} mutant fly (Fig 3B–D). A large increase in interommatidial cell number and massive eye overgrowth were seen for both *mer*; $mtm^{\Delta N}$ and *mer*; $mtm^{\Delta C}$ double mutant flies (Fig 3E–G and J–L), and for $mtm^{\Delta N}$, ex and $mtm^{\Delta C}$, ex double mutant flies (Fig 3M and N; Appendix Fig S3A and B). In addition, both $mtm^{\Delta N}$ and $mtm^{\Delta C}$ alleles led to mild increases in Hippo pathway target gene *diap1* and *ex* expressions (Appendix Fig S3C–F). The greatest increase in *diap1* and *ex* expression was seen in *mer*; $mtm^{\Delta N}$ and *mer*; $mtm^{\Delta C}$ double mutant flies (Fig 3H and I; Appendix Fig S3G and H). Taken together, these results suggest that both PH-GRAM domain and phosphatase domain are required for Mtm's function in growth suppression.

Mtm-mediated PI(3)P dynamics is critical for its function in growth suppression

Mtm is a phosphatidylinositide-3-phosphatase highly specific and efficient for the turnover of PI(3)P (Appendix Fig S4A), a lipid second messenger greatly enriched in the early endosome and actively involved in vesicular trafficking and cell signaling (Taylor *et al*, 2000; Marat & Haucke, 2016). The PH-GRAM domain of Mtm is a substrate binding domain for phospholipids, and the phosphatase domain is an enzymatically functional domain for dephosphorylation of its substrates at the D3 position (Begley *et al*, 2003). Since both domains are necessary for Mtm in growth suppression, we asked whether Mtm regulates tissue growth through controlling membrane phospholipid dynamics. Mtm has been reported to control PI(3)P dynamics in cell culture (Velichkova *et al*, 2010). Whether Mtm regulates membrane PI(3)P dynamics *in vivo* has not been shown. We therefore first examined PI(3)P level in flies containing *mtm* mutant tissue using a PI(3)P reporter 2xFYVE-GFP

Figure 2. Mtm functions synergistically with Hippo pathway in growth control.

A–J Images of representative adult eyes containing indicated mutant clones. Note the massive eye tissue overgrowth produced by *mer;mtm*, *ex,mtm*, *ft,mtm* or *mtm; kibra* double mutants. (A'-J') Mid-pupal eye discs of the indicated genotypes were stained for Dlg. The average numbers of extra interommatidial cells per ommatidium in respective genotypes were shown in the upper right corners. 10 ommatidia from different clone regions in each genotype were used for the quantification. Scale bars = 10 μm.

K–P Images of representative nota of adult flies containing indicate mutant clones. Note the massive overgrowth (circled area) in *ex,mtm* (O) or *ft,mtm* (P) double mutant flies.

Q, R Third instar eye discs containing *mer;mtm* double mutant clones (marked by the absence of GFP) were stained for Diap1 and Ex. Note the strong upregulations of Diap1 and Ex in the *mer;mtm* double mutant clones. Scale bars = 20 μm.

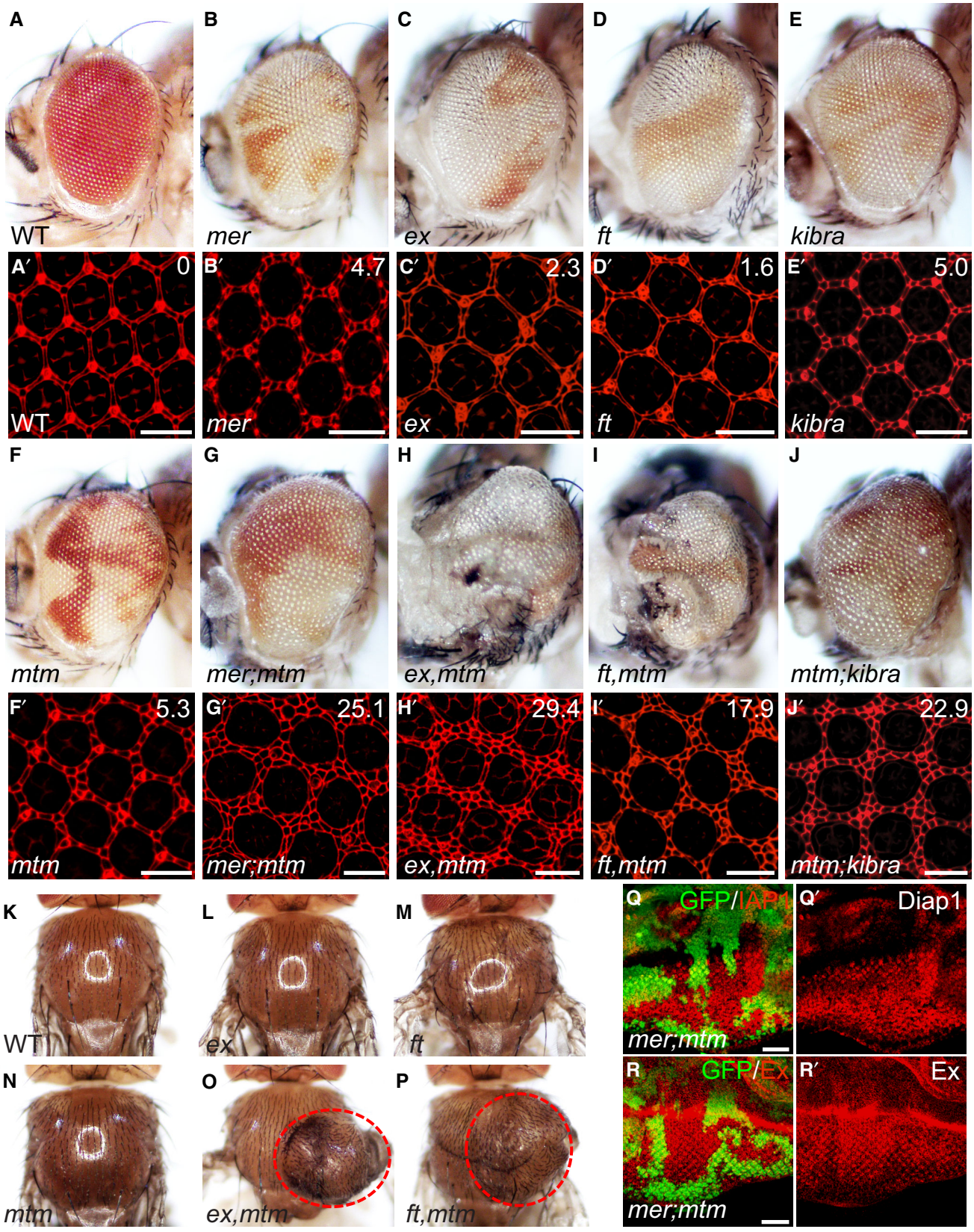
A
B
C
D
E
WT
mer
ex
ft
kibra
A′ 0
B′ 4.7
C′ 2.3
D′ 1.6
E′ 5.0
WT
mer
ex
ft
kibra
F
G
H
I
J
mtm
mer;mtm
ex,mtm
ft,mtm
mtm;kibra
F′ 5.3
G′ 25.1
H′ 29.4
I′ 17.9
J′ 22.9
mtm
mer;mtm
ex,mtm
ft,mtm
mtm;kibra
K
L
M
WT
ex
ft
N
O
P
mtm
ex,mtm
ft,mtm
Q GFP/IAP1
Q′ Diap1
mer;mtm
R GFP/Ex
R′ Ex
mer;mtm

Figure 2.

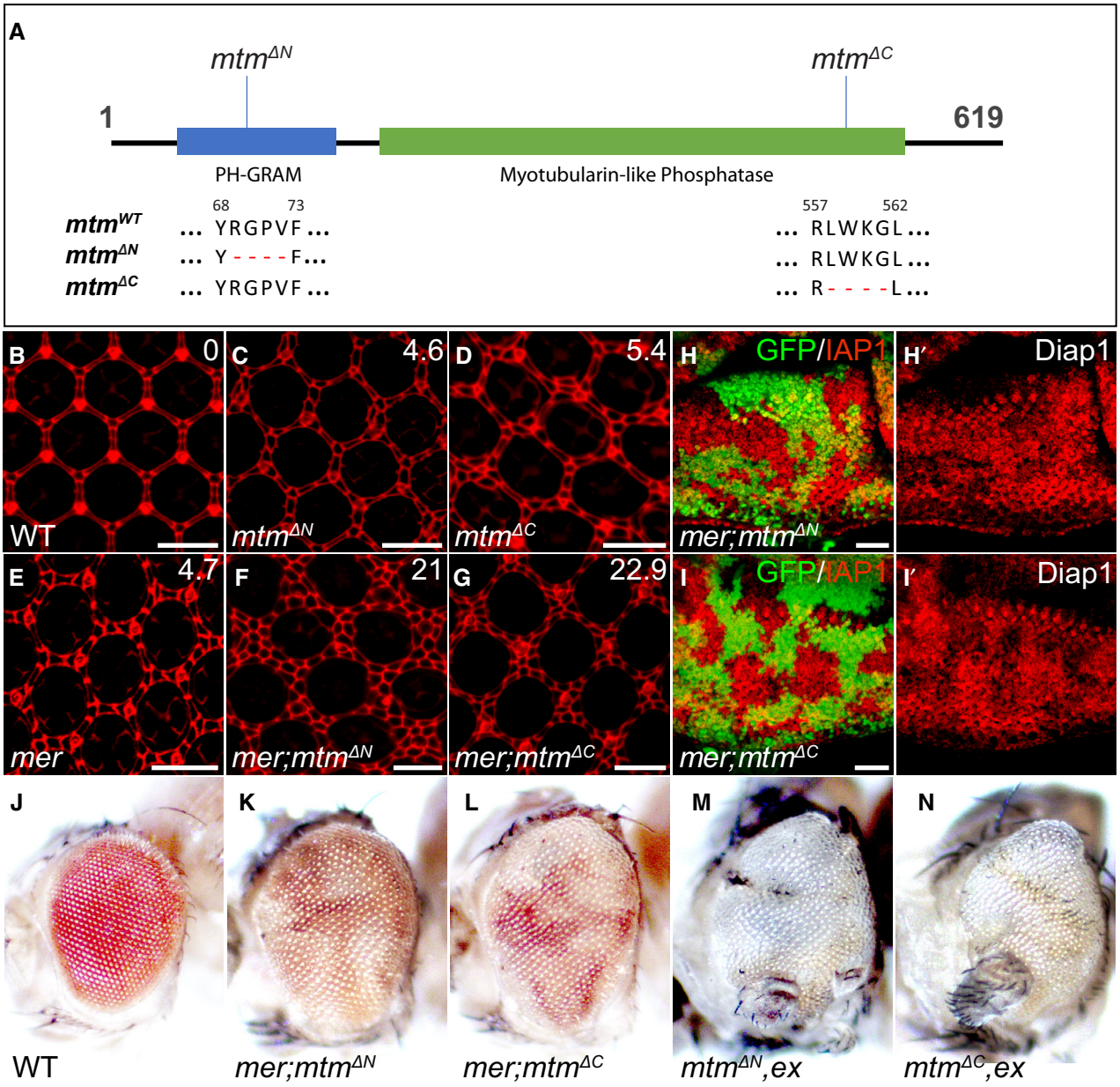

Figure 3. Mtm's growth suppression function requires both PH-GRAM domain and phosphatase domain.

A Schematic diagram of *Drosophila* Mtm protein domains. Domain-specific mutant alleles are indicated. Sequence alignment of the wild-type *mtm* (mtm^{WT}) and the two domain-specific *mtm* mutant alleles ($mtm^{\Delta N}$ and $mtm^{\Delta C}$) are shown below. The red "-" indicates deleted amino acid in the mutants.

B–G Mid-pupal eye discs of the indicated genotypes were stained for Dlg. The average numbers of extra interommatidial cells per ommatidium in each genotype were shown in the upper right corners. 10 ommatidia from different clone regions in each genotype were used for the quantification. Both $mtm^{\Delta N}$ and $mtm^{\Delta C}$ caused similarly increased numbers of interommatidial cells and synergistically interacted with *mer*. Scale bars = 10 μm.

H, I Third instar larval eye discs containing $mer;mtm^{\Delta N}$ or $mer;mtm^{\Delta C}$ double mutant clones (marked by the absence of GFP) were stained for Diap1. Note the strong upregulations of Diap1 in the double mutant clones. Scale bars = 20 μm.

J–N Images of representative adult eyes containing indicated mutant clones. Note the massive eye overgrowth produced by $mer;mtm^{\Delta N}$, $mer;mtm^{\Delta C}$, $mtm^{\Delta N}$,*ex* or $mtm^{\Delta C}$,*ex* double mutants.

(Gillooly *et al*, 2000). The FYVE-GFP reporter has been widely used to semi-quantitate PI(3)P level in cells (Lorenzo *et al*, 2006; Velichkova *et al*, 2010; Ketel *et al*, 2016) and its specificity for detecting PI(3)P *in vivo* was further confirmed (Appendix Fig S4B–D). Indeed, strong increases in the FYVE-GFP reporter were detected in *mtm* mutant clones in imaginal discs (Fig 4A–C) and follicle cells (Appendix Fig S4E), confirming the critical role of Mtm in maintaining PI(3)P dynamics *in vivo*. The increased PI(3)P in *mtm* mutant clones suggests that Mtm may regulate tissue growth through controlling PI(3)P dynamics. To test this hypothesis, we investigated

whether loss-of-*mtm*-induced overgrowth can be counteracted by manipulating the PI(3)P level. If the overgrowth phenotype seen in *mtm* mutant tissue results from increased PI(3)P production, reducing the PI(3)P level should suppress the overgrowth induced by loss-of-*mtm*. In *Drosophila*, there are three classes of phosphatidylinositol 3-kinases (PI3Ks) for PI(3)P synthesis, with class II

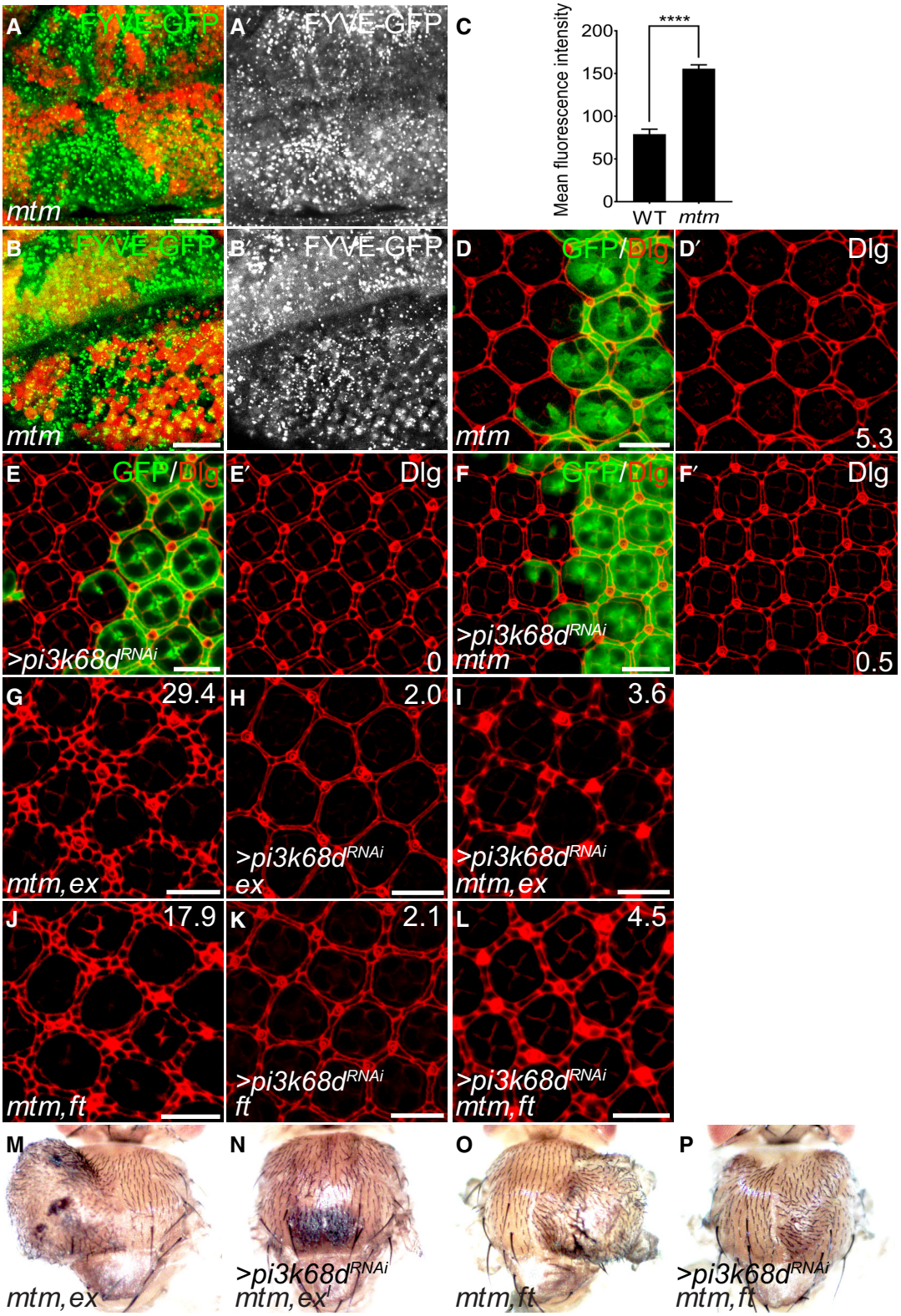

Figure 4.

Figure 4. Mtm-mediated PI(3)P dynamics is critical for its function in growth suppression.

A–C PI(3)P expression levels detected by a 2xFYVE-GFP reporter in a third instar larval wing disc (A) and eye disc (B) containing *mtm* mutant clones (marked by the absence of RFP). Quantification of the mean FYVE-GFP fluorescence intensity of *mtm* mutant clones and surrounding wild-type (WT) cells are shown (C). In all, 10 different *mtm* clones and surrounding regions in three biological replicates were used for the analysis. Note the strong increases in PI(3)P levels in the *mtm* mutant clones. Data are shown as mean ± SEM, ****$P < 0.0001$, Student *t*-test. Scale bars = 10 μm.

D–F Pupal eye discs containing clones (GFP positive) of indicated genotypes were stained for Dlg. The average numbers of extra interommatidial cells per ommatidium in each genotype were shown in the lower right corners. 10 ommatidia from different clone regions in each genotype were used for the quantification. Note *pi3k68d* RNAi almost completely suppressed loss-of-*mtm*-induced extra interommatidial cells. Scale bars = 10 μm.

G–L Pupal eye discs of indicated genotypes were stained for Dlg. The average numbers of extra interommatidial cells per ommatidium in each genotype were shown in the upper right corners of each panel. 10 ommatidia from different clone regions in each genotype were used for the quantification. Note *pi3k68d* RNAi dramatically suppressed the interommatidial cell increases in the *mtm,ex* and *mtm,ft* double mutant flies. Scale bars = 10 μm.

M–P Images of representative adult fly nota containing indicated mutant clones. Note that the massive notum tissue overgrowth was largely suppressed by *pi3k68d* RNAi knockdown in *mtm,ex* or *mtm,ft* double mutant flies.

and class III PI3Ks being necessary for the accumulation of PI(3)P pools (Velichkova *et al*, 2010). *Pi3K68D* is the only class II PI3K, while *vps34* is the only class III PI3K. Strikingly, while knockdown of *Pi3K68D* by RNAi had no visible effect on interommatidial cells in pupal retina (Fig 4E), it completely suppressed *mtm* mutant-induced interommatidial cell number increase (Fig 4D and F). The results were further confirmed by two independent *Pi3K68D* RNAi lines (Appendix Fig S4G and H). Interestingly, knockdown of *vps34* had no apparent effect on suppressing the interommatidial cell increase caused by loss-of-*mtm* (Appendix Fig S4I and J). These results suggest that the class II PI3K Pi3K68D, but not the class III PI3K Vps34, antagonizes Mtm's function in growth control. RNAi knockdown of *Pi3K68D* also greatly rescued the large increase in interommatidial cell numbers (Fig 4G–L) and the massive overgrowth (Fig 4M–P) seen in *ex; mtm* and *ft; mtm* double mutant flies.

Since Mtm has been reported to regulate PI(3,5)P2 level in cells (Appendix Fig S4A) (Velichkova *et al*, 2010), we asked whether PI(3,5)P2 dynamics contribute to the observed overgrowth seen in *mtm* mutants. While we were not able to detect levels of PI(3,5)P2 *in vivo* due to the lack of specific probes, we found that RNAi knocking down Fab1, a *Drosophila* PI3P 5-kinase that phosphorylates PI3P to generate PI(3,5)P2, had no effect on the abnormal increase in interommatidial cell number in *mtm* mutant eyes (Appendix Fig S4K and L), suggesting that PI(3,5)P2 unlikely plays a role in Mtm growth control function. In addition to PI(3,5)P2, we further examined whether Mtm regulates the dynamics of PI(4)P and PI(4,5)P2, two membrane lipids with reported function in regulating Hippo signaling (Yan *et al*, 2011; Chinthalapudi *et al*, 2018; Hong *et al*, 2020). We did not see detectable changes for PI(4)P (Appendix Fig S5A and B) and PI(4,5)P2 (Appendix Fig S5D and E) levels in *mtm* mutant clones, monitored by Osh2PH-GFP and PLCδ-PH-GFP reporters (Appendix Fig S5C), respectively. In addition, we found no apparent rescue of loss-of-*mtm*-caused extra interommatidial cells with RNAi knockdown of PI4KIIIα (Appendix Fig S5F) *or* Sktl (Appendix Fig S5G), two kinases required for PI(4)P and PI(4,5)P2 productions, respectively. Taken together, the data suggest that Mtm-mediated PI(3)P dynamics is critical for its function in growth suppression.

Mtm regulates F-actin dynamics and actomyosin activity

Mtm has been suggested to regulate cortical actin cytoskeleton remodeling in *Drosophila* hemocytes (Velichkova *et al*, 2010). We therefore asked whether Mtm regulates F-actin during fly development. Indeed, we found that loss-of-*mtm* caused a strong F-actin accumulation in eye discs (Fig 5A), supporting the important *in vivo* function of Mtm in F-actin remodeling. Importantly, while RNAi knockdown of Pi3K68D itself has no detectable effect on F-actin (Appendix Fig S6A), it largely abolished loss-of-*mtm*-induced F-actin accumulation, suggesting Mtm modulates F-actin through regulating PI(3)P level (Fig 5B).

F-actin is a major component of the actomyosin cytoskeleton, and actomyosin-mediated cytoskeletal tension plays an important role in regulating the Hippo pathway (Zhao *et al*, 2012; Sun &

Figure 5. Mtm controls tissue growth through regulating actomyosin activity.

A F-actin visualization in a third instar larval eye disc containing *mtm* mutant clone (GFP positive) by phalloidin. Note the strong increase in F-actin staining in the *mtm* clone. Scale bar = 20 μm.

B A third instar larval eye disc containing *pi3k68d* RNAi-overexpressing *mtm* mutant clones (GFP positive) was stained for F-actin. Note the strong rescue of loss-of-*mtm*-induced F-actin accumulation by *pi3k68d* RNAi knockdown. Scale bar = 20 μm.

C–G Pupal eye discs containing clones (GFP positive) of indicated genotypes were stained for phospho-MLC (p-MLC). Note the increased p-MLC in *mtm* mutant clones (D) and coexpressing *pi3k68d* RNAi suppressed the observed p-MLC increase (E). Also, note that the RNAi knockdown of Rok decreased p-MLC staining (F) and rescued the upregulation of p-MLC (G) induced by loss-of-*mtm* (G). Scale bars = 10 μm.

H, I Pupal eye discs containing clones (GFP positive) of indicated genotypes were stained for Dlg. The average numbers of extra interommatidial cells per ommatidium in each genotype were shown in the lower right corners. 10 ommatidia from different clone regions in each genotype were used for the quantification. Note *rok* RNAi almost completely suppressed loss-of-*mtm*-induced extra interommatidial cells. Scale bars = 10 μm.

J–O Pupal eye discs of indicated genotypes were stained for Dlg. The average numbers of extra interommatidial cells per ommatidium in each genotype were shown in the lower right corners. 10 ommatidia from different clone regions in each genotype were used for the quantification. Note Rok RNAi knockdown largely suppressed the extra interommatidial cells seen in the *mtm,ex* and *mtm,ft* double mutant flies. Scale bars = 10 μm.

P–S Images of representative adult fly nota containing indicated mutant clones. Note that the massive notum tissue overgrowth seen in the *mtm,ex* double mutant flies was largely rescued by *rok* RNAi.

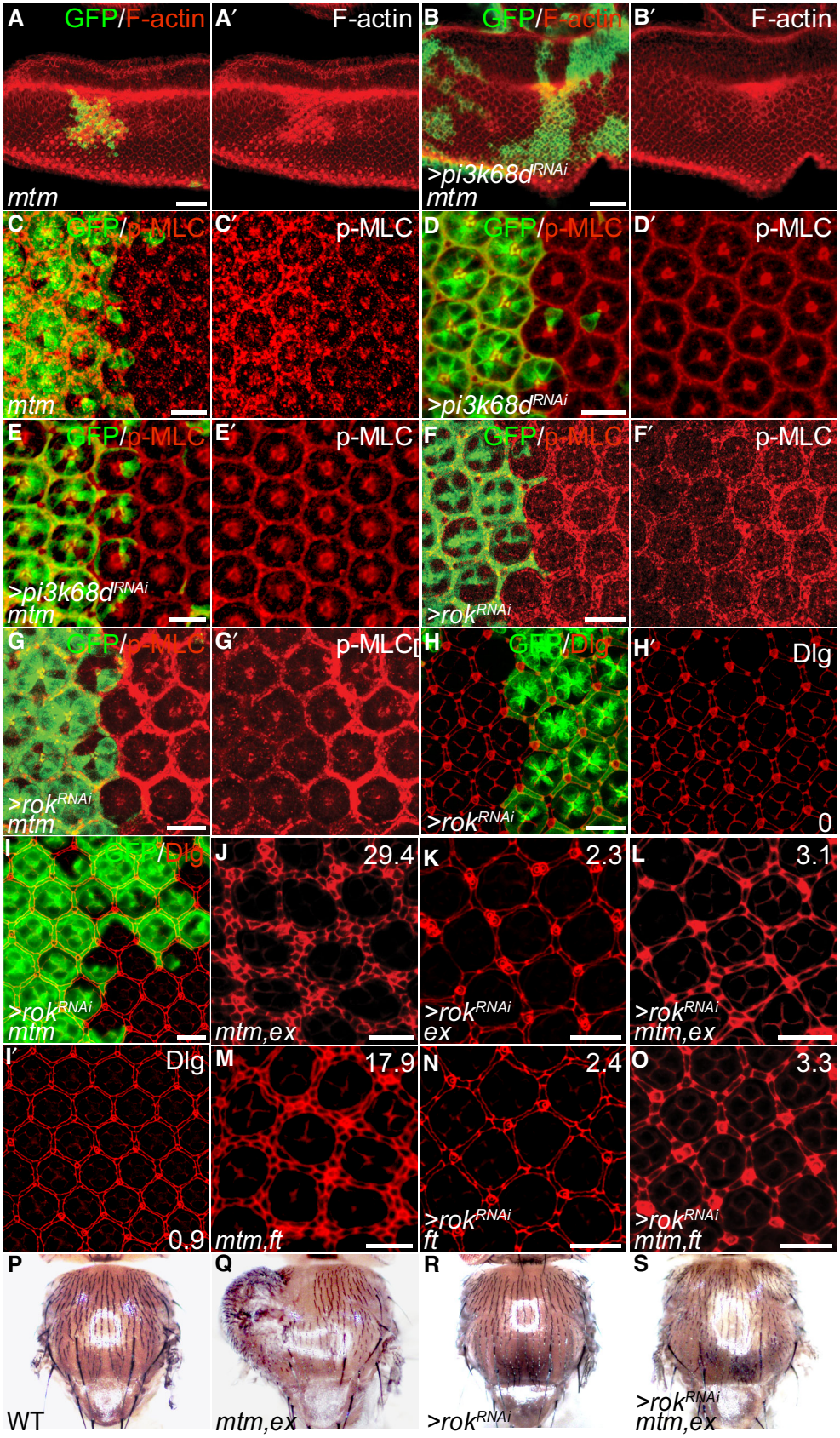

Figure 5.

Irvine, 2016). The strong accumulation of F-actin in *mtm* mutant clones prompted us to investigate whether Mtm regulates actomyosin activity. The non-muscle myosin II is a major mediator of cytoskeletal tension regulated Hippo signaling (Rauskolb *et al*, 2014; Deng *et al*, 2015). Its activity is regulated by phosphorylation of the light chain of myosin II (MLC) (Vicente-Manzanares *et al*, 2009). We therefore examined the activity of non-muscle myosin II by detecting the phosphorylation of the light chain of myosin II (MLC) (Vicente-Manzanares *et al*, 2009). Interestingly, we found increased p-MLC in mtm mutant cells in both pupal eye disc (Fig 5C) and third instar larva wing disc (Appendix Fig S6B), suggesting Mtm regulates actomyosin activity. To test whether loss-of-*mtm* affects the basal level of MLC, we examined the expression of a mCherry reporter driven by *spaghetti squash* (*sqh*), the gene encoding MLC in *Drosophila*, in *mtm* mutant cells. We noticed mild upregulation of mCherry expression in the *mtm* mutant tissue (Appendix Fig S6C), suggesting that Mtm regulates actomyosin activity by affecting both MLC basal expression and phosphorylation levels. To investigate whether Mtm-mediated PI(3)P is critical in this process, we knocked down Pi3K68D in *mtm* mutant clones and examined p-MLC level. While RNAi knockdown of Pi3K68D had no detectable effect on p-MLC (Fig 5D), it completely suppressed elevated p-MLC in *mtm* mutant cells (Fig 5E).

Taken together, these results suggest that Mtm regulates F-actin dynamics and actomyosin activity through PI(3)P dynamics.

Myosin activity but not increased F-Actin accumulation is critical for tissue overgrowth induced by loss-of-*mtm*

F-actin and myosin are well recognized as important regulators of tissue growth in the Hippo pathway in both *Drosophila* and mammalian systems (Boggiano & Fehon, 2012; Matsui & Lai, 2013; Gaspar & Tapon, 2014; Sun & Irvine, 2016; Seo & Kim, 2018). We therefore asked whether Mtm mediates tissue growth through F-actin, myosin, or both.

First, we eliminated F-actin accumulation in *mtm* mutant clones by RNAi knocking down Arpc1, an important component of Arp2/3 complex required for F-actin polymerization (Fig EV1C). Interestingly, while F-actin accumulation was entirely suppressed in *mtm* mutant clones overexpressing *arpc1 RNAi* (Fig EV1A–C), no rescue of extra interommatidial cells was found (Fig EV1D and E), suggesting the observed F-actin accumulation is dispensable for *mtm* mutant overgrowth. More interestingly, we found that p-MLC remained elevated in *mtm* mutant clones overexpressing *arpc1 RNAi* (Fig EV1F and G), suggesting decoupled regulation of F-actin dynamics and myosin activity by Mtm. This finding is consistent with a previous report that loss-of-*spectrin* activates myosin and inhibits Hippo signaling without affecting the actin cytoskeleton (Deng *et al*, 2015) and is supported by our observation that loss-of-*hpo* led to strong F-actin accumulation but normal MLC activity (Fig EV1H and I).

Next, we asked whether myosin activity is critical for Mtm in regulating tissue growth and the Hippo pathway. The phosphorylation of MLC is mediated by multiple kinases in *Drosophila*, including Rho-associated protein kinase (Rok) (Vicente-Manzanares *et al*, 2009; Deng *et al*, 2015; Xu *et al*, 2018). As expected, knockdown of Rho kinase (Rok) by RNAi effectively inhibited actomyosin activity, evidenced by decreased p-MLC level (Fig 5F). Strikingly, loss-of-*mtm*-induced p-MLC and interommatidial cell number increases were entirely suppressed by *rok* RNAi (Fig 5G–I). RNAi knockdown of *sqh* also largely suppressed *mtm* mutant-induced interommatidial cell number increase (Appendix Fig S6D and E). Taken together, these results suggest that myosin activity but not the increased F-actin accumulation is critical for loss-of-*mtm*-induced overgrowth.

Having established actomyosin as the major downstream effector of Mtm in growth control, we next examined whether actomyosin mediates the synergistic interactions between Mtm and Hippo pathway upstream regulators. Indeed, RNAi knockdown of *rok* largely suppressed the massive extra interommatidial cells seen in *ex*, *mtm* and *ft*, *mtm* double mutant clones (Fig 5J–O). Consistent with the suppression of extra interommatidial cells, *rok* RNAi also inhibited the massive tissue overgrowth seen in the adult nota of *mtm*, *ex* double mutant flies (Fig 5P–S). These results suggest that actomyosin mediates the synergistic interactions between Mtm and Hippo pathway.

We have shown that RNAi knockdown of Mtm expression in Kc167 cells led to decreased Yki phosphorylation. To answer the question of whether Mtm regulates Yki phosphorylation through actomyosin, we treated Kc167 cells with LatB and examined the effect of Mtm RNAi knockdown on LatB-induced Yki phosphorylation. Surprisingly, we found that RNAi knockdown of Mtm largely inhibited LatB-induced Yki phosphorylation in Kc167 cells (Appendix Fig S6F). Since LatB treatment leads to depolymerization of F-actin and subsequent disruption of actomyosin cytoskeleton, the inhibition of LatB-induced Yki phosphorylation by Mtm RNAi in Kc167 cells is unlikely actomyosin dependent. This result therefore suggests that Mtm may have actomyosin independent function in regulating Hippo signaling in Kc167 cells.

Rab11 mediates Mtm-regulated actomyosin activity and tissue growth

Mtm is an inositol phosphatase highly efficient for dephosphorylation of PI(3)P, which is greatly enriched in the early endosome, where it serves as a binding platform to recruit effector proteins such as early endosome antigen 1 and Rabenosyn-5 to instruct proper endosomal transport, fusion, and maturation (Simonsen *et al*, 1998; Gillooly *et al*, 2000; Nielsen *et al*, 2000; Lindmo & Stenmark, 2006; Robinson & Dixon, 2006; Balla, 2013). During this process, the Rab GTPases such as Rab5 and Rab7 play essential roles in assisting the membrane localization of the effector proteins (Simonsen *et al*, 1998; Nielsen *et al*, 2000; Stenmark, 2009). Abnormal elevation or deficiency of PI(3)P causes severe endosomal trafficking defects (Zoncu *et al*, 2009; Morel *et al*, 2013; Singla *et al*, 2019; Steinfeld *et al*, 2021). Therefore, we asked whether loss-of-*mtm* leads to endosomal trafficking defects and, if so, whether such defects account for the elevated actomyosin activity seen in *mtm* mutants. To answer these questions, we first examined the expression of two key components of endocytic trafficking: Rab5, an early endosome marker, and Rab7, a late endosome marker, in *mtm* mutant clones. Interestingly, we found dramatic accumulations of both Rab5 and Rab7 in *mtm* mutant cells (Fig EV2A and B), suggesting defects of endocytic trafficking. The defective vesicular trafficking was further confirmed by a transferrin endocytosis uptake assay showing a strong accumulation of intracellular transferrin in *mtm* mutant follicle cells (Fig EV2L).

To determine the role of Rab5 and Rab7 in loss-of-*mtm*-induced tissue growth, we manipulated the activities of Rab5 and Rab7 in *mtm* mutant clones and examined the interommatidial cell number changes. We found that overexpression of a dominant negative form of Rab5, $Rab5^{S43N}$, or a constitutively active form of Rab5, $Rab5^{Q88L}$, in *mtm* mutants still induced obvious extra interommatidial cells (Fig EV2C and D). Similarly, overexpression of a dominant negative form of Rab7, $Rab7^{T22N}$ (Fig EV2E), or a constitutively active form of Rab7, $Rab7^{Q67L}$ (Fig EV2F), in *mtm* mutants induced a comparable amount of extra interommatidial cells as *mtm* single mutant tissue did. These results suggest Rab5 and Rab7 may not be directly involved in Mtm deficiency-mediated tissue overgrowth.

In addition to early and late endocytosis represented by Rab5 and Rab7, respectively, the Rab11 GTPase is actively involved in exocytosis and endocytic recycling. Rab11 activation plays a critical role in maintaining proper plasma membrane dynamics and identities. Recent work in mammalian cells demonstrated that spatially regulated PI(3)P turnover is associated with Rab11 activation and subsequent release of recycling cargos from endosomes (Jean *et al*, 2012; Campa *et al*, 2018). Interestingly, MTM1, another mammalian homolog of Mtm, has been shown to control PI(3)P hydrolysis and associated Rab11 activity (Campa *et al*, 2018). We therefore reasoned that the long-lasting accumulation of PI(3)P in *mtm* mutant tissue may fail to maintain proper Rab11 activity, leading to cellular trafficking defects and tissue overgrowth seen in *mtm* mutant flies. To test this hypothesis, we first examined the level of Rab11 in *mtm* mutant clones. We found that Rab11 accumulated in *mtm* mutant clones (Fig 6A), indicating Rab11 functional defects. To further investigate the role of Rab11 in loss-of-*mtm*-induced growth defects, we first overexpressed a dominant negative form of Rab11, $Rab11^{S25N}$, in *mtm* mutant tissues and investigated its effect on loss-of- *mtm*-induced tissue overgrowth. Overexpression of $Rab11^{S25N}$ in *mtm* mutant pupal retina produced many more extra interommatidial cells than the *mtm* single mutant did (Fig 6B and C). Next, we tested the effect of overexpression of a constitutively active form of Rab11, $Rab11^{Q70L}$, in *mtm* mutant tissues. Strikingly, overexpression of $Rab11^{Q70L}$ completely rescued the extra interommatidial cells seen in *mtm* mutant pupal retina (Fig 6D). Importantly, overexpression of $Rab11^{Q70L}$ itself had no visible effect on pupal retina interommatidial cells (Fig EV2G). Furthermore, we found that overexpression of $Rab11^{Q70L}$ almost completely blocked the increase in p-MLC (Fig 6E and F) and the accumulations of F-actin (Fig EV2I and J) in *mtm* mutant tissues. These results suggest that loss-of-*mtm*-induced actomyosin activity and tissue overgrowth are caused by impaired Rab11 activity. To further confirm the idea, we tested whether overexpression of a dominant negative Rab11, $Rab11^{S25N}$, shows similar growth regulatory defects and actomyosin activity as loss-of-*mtm*. If loss-of-*mtm* functions through inactivating Rab11 to enhance actomyosin activity and induce tissue overgrowth, overexpression of $Rab11^{S25N}$ should phenocopy the effects of Mtm depletion. Indeed, overexpression of $Rab11^{S25N}$ induced an increase in interommatidial cells (Fig 6G) and p-MLC level in the pupal retinas (Fig 6H), and F-actin accumulation in eye disc (Fig EV2K), similar to that seen in *mtm* mutant tissues.

Taken together, these results suggest that Rab11 activity mediates Mtm's regulatory function of actomyosin activity and tissue growth. Interestingly, overexpression of $Rab11^{Q70L}$ showed no obvious effect on accumulations of Rab5 and Rab7 in the *mtm* mutant tissues (Fig EV3A–D), which, however, were completely blocked by Pi3K68D RNAi (Fig EV3E and F), suggesting that Rab5 and Rab7 endosomal accumulations result from PI(3)P increase. In addition, accumulation of Rab11 in *mtm* mutant tissues was also completely blocked by Pi3K68D RNAi (Fig EV3G and H), indicating that Rab11 functional defects are results of abnormal PI(3)P elevation.

Having established Rab11 as a key functional link between PI(3)P and actomyosin in Mtm-mediated tissue growth control, we next examined whether Rab11 mediates the synergistic interactions between Mtm and Hippo pathway regulators. Indeed, $Rab11^{Q70L}$ overexpression largely suppressed the massive extra interommatidial cells seen in *ex*,*mtm* and *ft*,*mtm* double mutant pupal retina (Fig 6I–N). Consistently, while overexpression of $Rab11^{Q70L}$ alone did not induce abnormal tissue growth, it completely inhibited the massive tissue overgrowth of *mtm*, *ex* and *mtm*, *ft* double mutant flies (Fig 6O–T). We also found dramatically increased interommatidial cells in *mer; UAS-*$Rab11^{S25N}$ and *ex; UAS-*$Rab11^{S25N}$ double mutant clones (Fig EV2M and N), further supporting that Rab11

Figure 6. Rab11 mediates Mtm-regulated actomyosin activity and tissue growth.

A A third instar larval eye disc containing *mtm* mutant clones (marked by the absence of GFP) was stained for Rab11. Note the increase in Rab11 staining in *mtm* mutant clones. Scale bar = 20 μm.

B–D Pupal eye discs containing clones (GFP positive) of indicated genotypes were stained for Dlg. The average numbers of extra interommatidial cells per ommatidium in different genotypes were shown in the lower right corners. 10 ommatidia from different clone regions in each genotype were used for the quantification. Note coexpression of the dominant negative Rab11, $Rab11^{S25N}$, increased the extra interommatidial cells in *mtm* mutant tissue (C) while coexpression of the constitutively active Rab11, $Rab11^{Q70L}$, almost completely rescued the extra interommatidial cells in *mtm* mutant tissue (D). Scale bars = 10 μm.

E, F Pupal eye discs containing clones (GFP positive) of indicated genotypes were stained for p-MLC. Note that $Rab11^{Q70L}$ coexpression largely suppressed the p-MLC upregulation induced by loss-of-*mtm*. Scale bars = 10 μm.

G Pupal eye disc containing clones (GFP positive) overexpressing the dominant negative Rab11 was stained for Dlg. The average number of extra interommatidial cells per ommatidium in the clones was shown in the lower right corner. 10 ommatidia from different clone regions were used for the quantification. Note the overexpression of the dominant negative Rab11, $Rab11^{S25N}$, increased a similar amount of extra interommatidial cells as that seen in *mtm* mutant tissue. Scale bar = 10 μm.

H Pupal eye disc containing clones (GFP positive) overexpressing the dominant negative Rab11 was stained for p-MLC. Note that $Rab11^{S25N}$ overexpression mildly promoted the p-MLC upregulation. Scale bar = 10 μm.

I–N Pupal eye discs of indicated genotypes were stained for Dlg. The average numbers of extra interommatidial cells per ommatidium in each genotype were shown in the lower right corners. 10 ommatidia from different clone regions in each genotype were used for the quantification. Note overexpression of $Rab11^{Q70L}$ largely suppressed the extra interommatidial cells seen in the *mtm*,*ex* or *mtm*,*ft* double mutant flies (K and N). Scale bars = 10 μm.

O–T Images of representative adult fly nota containing indicated mutant clones. Note that the massive notum tissue overgrowth seen in *mtm*,*ex* (P) or *mtm*,*ft* (Q) double mutant flies was largely suppressed by $Rab11^{Q70L}$ co-expression.

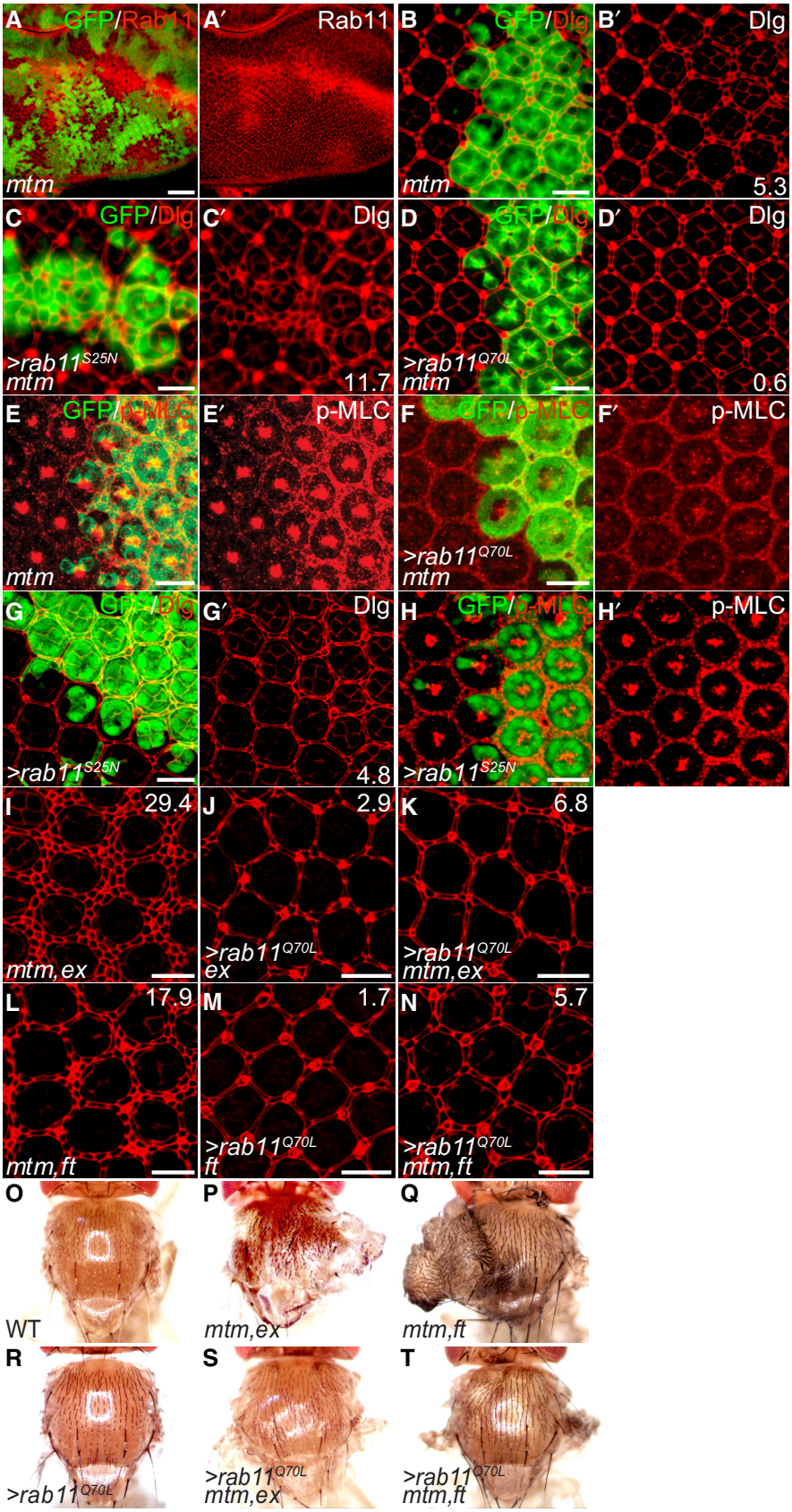

Figure 6.

mediates the synergistic interactions between Mtm and Hippo pathway regulators.

Mtm regulates multiple membrane-associated proteins

Rab11-mediated vesicular trafficking is important in maintaining plasma membrane integrity, including the proper distribution of various membrane-associated proteins. Interestingly, we found a strong accumulation of Rho1, a key regulator that activates non-muscle myosin-II through Rok kinase, in *mtm* mutant follicle cells (Fig EV4A). In particular, the Rho1 accumulation is most obvious at apical lateral junctions and apical cortex in *mtm* mutant follicle cells (Fig EV4A). The Rho1 accumulation was also observed in $Rab11^{S25N}$ overexpression follicle cells (Fig EV4B), further suggesting Rab11 activity is critical for proper Rho1 expression and localization. The observed Rho1 accumulation in *mtm* mutant cells was completely suppressed by $Rab11^{Q70L}$ overexpression (Fig EV4C), suggesting Rab11 dysfunction underlies *mtm* mutant-induced Rho1 abnormality. Importantly, RNAi knockdown of Pi3K68D completely suppressed abnormal Rho1 accumulation (Fig EV4D), suggesting a critical role of Mtm-mediated PI3P dynamics in Rho1 membrane distribution. To ask whether the observed accumulation of Rho1 is critical for Mtm in regulating tissue growth, we overexpressed Rho1 RNAi in *mtm* mutant cells. Strikingly, while overexpressing Rho1 RNAi completely suppressed Rho1 protein accumulation, it did not suppress the elevated p-MLC and the increased interommatidial cells of *mtm* mutants (Fig EV4E–G). Therefore, it is unlikely that Mtm regulates tissue growth through Rho1. Interestingly, we found that while Rho1 RNAi had no effect on p-MLC increase, it completely suppressed the F-actin accumulation in *mtm* mutant cells (Fig EV4H), suggesting Mtm may regulate F-actin remodeling through Rho1. This observation further supports our finding that F-actin accumulation induced by loss-of-*mtm* and actomyosin activation are decoupled.

Loss-of-*mtm* also promoted similar membrane accumulations of DE-cadherin (Fig EV5A), Armadillo (Fig EV5B), and aPKC (Fig EV5C). However, like Rho1 RNAi, knockdown of these membrane-associated proteins had no rescues on loss-of-*mtm*-induced tissue overgrowth (Fig EV5D–I), suggesting that the detected membrane protein accumulations are not critical for *mtm* mutant overgrowth.

Next, we examined the localization of several membrane-associated Hippo pathway components, including Ex, Merlin, Kibra, Crumbs, and α-Spectrin. We found that localizations of these proteins are not affected, although a mild accumulation of Ex at the apical membrane was found (Appendix Fig S7A–H). To test the possibility that the observed rescue with constitutively active $Rab11^{Q70L}$ may have resulted from increased apical Crumbs trafficking, we overexpressed $Rab11^{Q70L}$ in *mtm* mutant cells. We found no detectable changes in the level and the localization of Crumbs (Appendix Fig S7I). Co-deletion of Crumbs further enhanced *mtm* mutant overgrowth (Appendix Fig S7J and K), suggesting that Crumbs, like other upstream regulators, functions in parallel with Mtm in the Hippo pathway.

Together, these results suggest that Mtm-regulated various Rab11-dependent membrane proteins may not be directly involved in Mtm-mediated growth control.

Conserved function of human MTMR2

It has been reported that co-expression of myotubularin related protein-2 (MTMR2), the human orthologue of *Drosophila* Mtm, is able to rescue the lethality of *mtm* mutant flies, suggesting Mtm is functionally conserved in mammals (Velichkova *et al*, 2010). To further investigate whether MTMR2 has conserved function in growth control, we generated transgenic flies carrying full-length human MTMR2 cDNA. As reported, ectopic expression of MTMR2 fully rescued the lethality of the *mtm* mutant flies (Fig 7M). Importantly, we found that ectopic expression of MTMR2 fully inhibited the extra interommatidial cells caused by loss-of-*mtm* (Fig 7A and B). Moreover, co-expression of MTMR2 also largely suppressed the extra interommatidial cells (Fig 7C–F) and massive overgrowth seen in *ex*, *mtm* and *ft*, *mtm* double mutant flies (Fig 7G–L). These results, therefore, suggest that MTMR2 has conserved function in the Hippo pathway.

Mutations of the MTMR2 gene are major causes of CMT4B1 disease, a hereditary demyelinating neurodegenerative disorder characterized by focally folded myelin of the peripheral nerves in both

Figure 7. Conserved function of MTMR2 in tissue growth regulation.

A, B Pupal eye discs containing *mtm* mutant clones (GFP positive) with or without wild-type MTMR2 or disease-linked $MTMR2^{G103}$ co-expression were stained for Dlg. The average numbers of extra interommatidial cells per ommatidium in each genotype were shown in the lower right corners. 10 ommatidia from different clone regions in each genotype were used for the quantification. Note co-expression of the wild-type human MTMR2 almost completely suppressed loss-of-*mtm*-induced extra interommatidial cells. Scale bars = 10 μm.

C–F Pupal eye discs of indicated genotypes were stained for Dlg. The average numbers of extra interommatidial cells per ommatidium in each genotype were shown in the upper right corners of each panel. 10 ommatidia from different clone regions in each genotype were used for the quantification. Note co-expression of human MTMR2 greatly suppressed the massive extra interommatidial cells seen in the *mtm*,*ex* and *mtm*,*ft* double mutant flies. Scale bars = 10 μm.

G–L Images of representative adult fly nota containing indicated mutant clones. Note the massive notum tissue overgrowth seen in *mtm*,*ex* (H) or *mtm*,*ft* (K) double mutant flies was largely suppressed by MTMR2 co-expression.

M Rescue of *mtm* null mutant lethality by wild-type and disease-linked MTMR2. Expressions of the wild-type and disease-linked MTMR2 were driven by Tub-GAL4. Numbers (*n*) of progeny flies with the indicated genotypes were shown. The theoretical ratio between $mtm^{-/-}$ and $mtm^{-/+}$ progeny flies overexpressing MTMR2 should be 1:2. Note overexpression of the wild type MTMR2 completely rescued fly lethality caused by loss-of-*mtm* while overexpression of disease-linked MTMR2, $MTMR2^{G103}$, completely failed to rescue fly lethality.

N A pupal eye disc containing *mtm* mutant clone (GFP positive) with $MTMR2^{G103}$ co-expression were stained for Dlg. The average number of extra interommatidial cells per ommatidium in the clones was shown in the lower right corner of the panel. 10 ommatidia from different clone regions were used for the quantification. Note co-expression of $MTMR2^{G103}$ partially suppressed loss-of-*mtm*-induced extra interommatidial cells. Scale bar = 10 μm.

O–Q Pupal eye discs containing clones (GFP positive) of indicated genotypes were stained for p-MLC. Note the increased p-MLC was completely rescued by MTMR2 but not $MTMR2^{G103E}$ co-expression in *mtm* mutant clone. Scale bar = 10 μm.

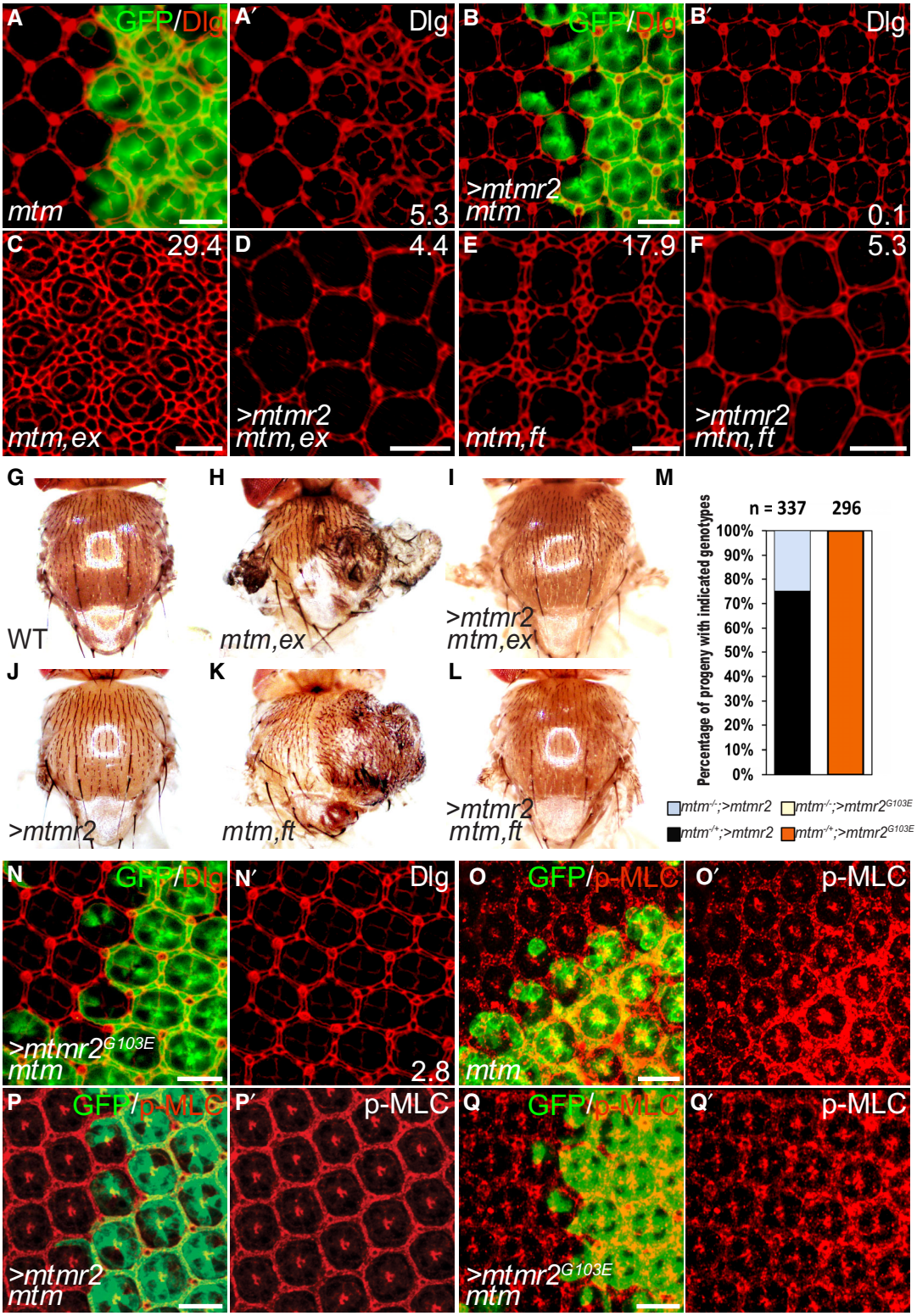

Figure 7.

human and mouse models (Bolino *et al*, 1996, 2000; Bonneick *et al*, 2005). To explore the underlying pathogenesis of CMT4B1, we generated a transgenic fly carrying a disease-linked MTMR2 mutation, $MTMR2^{G103E}$, a mutation identified in a family of English origin that caused typical CMT4B1 symptoms (Houlden *et al*, 2001). Consistent with its reported low catalytic activity (Berger *et al*, 2002), $MTMR2^{G103E}$ co-expression failed to rescue the lethality of *mtm* mutant flies (Fig 7M). We then examined whether overexpression of

MTMR2^{G103E} can rescue the growth defects seen in *mtm* mutant pupal retina. Interestingly, unlike a complete rescue by wild-type MTMR2 overexpression, *MTMR2*^{G103E} overexpression only partially rescued the increased interommatidial cells caused by *mtm* loss-of-function (Fig 7N). Next, we compared the effects of overexpressing wild-type MTMR2 vs. *MTMR2*^{G103E} mutant on loss-of-*mtm* induced cellular defects, including endocytic trafficking impairments, F-actin accumulation, and p-MLC increase. Strikingly, co-expression of wild-type MTMR2 fully rescued the Rab5 (Appendix Fig S8A and B), Rab7 (Appendix Fig S8D and E), and Rab11 (Appendix Fig S8G and H) accumulations, F-actin enrichment (Appendix Fig S8J and K), and p-MLC elevation (Fig 7O and P) in *mtm* mutant clones, demonstrating the cellular function of MTMR2 in the regulation of endocytic trafficking and actomyosin activity is conserved. However, co-expression of *MTMR2*^{G103E} only partially rescued loss-of-*mtm*-induced Rab5 (Appendix Fig S8C), Rab7 (Appendix Fig S8F), and Rab11 (Appendix Fig S8I) accumulations, F-actin enrichment (Appendix Fig S8L), and p-MLC elevation (Fig 7Q). The incomplete rescue of *mtm* mutant cellular function by *MTMR2*^{G103E} familiar mutation suggests that defects in endocytic trafficking and subsequent F-actin remolding and actomyosin activation contribute to the underlying pathogenesis of CMT4B1 disease.

Discussion

The Hippo pathway has emerged as a key signaling pathway that controls organ size in both flies and mammals (Pan, 2010; Halder & Johnson, 2011; Harvey & Hariharan, 2012; Yu *et al*, 2015; Kim & Jho, 2018; Misra & Irvine, 2018). Despite the well-studied core kinase cascade and the downstream transcriptional machinery, the upstream regulation of the Hippo pathway remains less understood. Accumulating evidence suggests the involvement of membrane phospholipids in Hippo pathway upstream regulation. The conformational change of the Hippo pathway upstream regulator Merlin (NF2 in human) is associated with membrane phosphatidylinositol 4,5-bisphosphate (PI(4,5)P2) binding (Chinthalapudi *et al*, 2018). The osmotic stress-induced PI(4,5)P2 enrichment at the plasma membrane is critical in NF2-mediated Hippo pathway activation (Hong *et al*, 2020). Through direct lipid–protein binding, the phosphatidic-acid-related lipid signaling functions as a key regulator of the Hippo pathway (Han *et al*, 2018). In *Drosophila*, the phosphatidylinositol 4-kinase (PI4KIIIalpha), a PI4-kinase that catalyzes the production of PI(4)P, is required in follicle cells for Merlin apical localization and Hippo signaling activation (Yan *et al*, 2011). In this study, we identified the phosphatidylinositol-3-phosphatase, Mtm, as a novel upstream regulator of the Hippo pathway. Mtm has known function in controlling phosphatidylinositol 3-phosphate (PI(3)P) dynamics (Velichkova *et al*, 2010). Importantly, the RNAi knockdown of Pi3K68D, the class II PI3-kinase known for the production of PI(3)P, suppressed loss-of-*mtm*-induced growth defects and largely inhibited the synergistic interactions seen between Mtm and multiple Hippo pathway upstream regulators. Therefore, our study suggests a critical role of the membrane lipid PI(3)P in Hippo pathway regulation and provides a novel functional link between membrane lipid dynamics and growth control.

Our study also shows that PI(3)P dynamics is a novel mode of upstream regulation of the actomyosin cytoskeleton in the Hippo signaling pathway. The actomyosin skeleton is known to serve as a hub to relay multiple input signals to the Hippo pathway. However, little is known about its upstream regulation. Recent studies uncovered the spectrin-based membrane skeleton as an upstream regulator of actomyosin cytoskeleton to regulate Hippo pathway signaling and tissue growth (Deng *et al*, 2015, 2020; Fletcher *et al*, 2015). Here our work suggests that membrane PI(3)P dynamics regulate actomyosin activity and function as a novel upstream input of actomyosin in the Hippo pathway. The PI(3)P-mediated actomyosin activity is physiologically important in regulating Hippo signaling and tissue growth based on our finding that inhibition of actomyosin activity by knocking down either Pi3K68D (the kinase required for PI(3)P synthesize) or Rok (the kinase required for actomyosin activation) completely suppressed the growth defects in *mtm* single mutant flies and further, the synergistic massive tissue overgrowth of representative double mutant flies between *mtm* and Hippo pathway regulators *ex* and *ft*. Our work therefore uncovered membrane lipid dynamics, specifically PI(3)P dynamics, as a critical regulator of the actomyosin cytoskeleton in Hippo signaling and growth control.

The apical cytocortex of epithelial cells functions as a critical site for the Hippo signaling activation regulated by tension-sensing mechanisms and other upstream regulators (Rauskolb *et al*, 2014; Su *et al*, 2017). Our study suggests a model that Mtm regulates PI(3)P-associated Rab11 activity and subsequent actomyosin activity through Rab11-mediated vesicular trafficking. This model is supported by the finding that overexpression of a constitutively active form of Rab11 completely suppressed loss-of-*mtm*-caused cellular defects, including enhanced actomyosin activity and increased interommatidial cells. More convincing is that overexpression of a dominant negative form of Rab11 phenocopies the observed cellular defects of *mtm* mutant cells and the synergistic interactions between Mtm and upstream regulators of the Hippo pathway. It is worth noting that endocytosis defects have been reported in *Drosophila* for *mer;ex* and *hpo* mutant cells in multiple tissues (Maitra *et al*, 2006; Yu *et al*, 2008). It will be interesting to explore the regulatory relationship between Mtm-mediated vesicle trafficking and those mediated by known Hippo pathway regulators and further their respective cellular mechanisms in controlling Hippo signaling activity and tissue growth.

Two unknowns require further investigation to fully understand the function of Mtm in the Hippo pathway. First, the molecular mechanism of how Mtm regulates Rab11 activity remains unclear. The endocytic recycling pathway controls the plasma membrane content by regulating the recycling of cargo molecules from early endosomes to the cell surface, which requires the proper function of Rab11 for exocytosis and endocytic recycling (Ullrich *et al*, 1996; Campa & Hirsch, 2017). Our data suggest that Mtm-mediated PI(3)P dynamics are critical for Rab11 function. Consistently, it has been reported that the transport of cargo molecules from peripheral early endosomes to perinuclear endocytic recycling compartments requires the proper level of PI(3)P and activation of Rab11 (Franco *et al*, 2014; Campa *et al*, 2018). Deficiency of PI(3)P level resulting from depletion of PI3K-C2α was reported to cause mislocalization and functional inactivation of Rab11, leading to primary cilium elongation defects in the mouse embryonic fibroblasts (Franco *et al*, 2014). Our study shows that excess PI(3)P resulting from *mtm* loss-of-function leads to accumulation and likely functional impairment

of Rab11, leading to enhanced actomyosin activity and tissue overgrowth. Thus, it seems that Rab11 functional activity requires proper amount of PI(3)P. Whereas excessive or deficient amounts of PI(3)P may lead to improper regulation of Rab11 activities. It will be interesting to investigate exactly how PI(3)P dynamics mediate Rab11 activity and subsequent cellular function in the Hippo pathway.

Additionally, it is unclear how Rab11 mediates the function of Mtm in the Hippo pathway and growth control. Our study suggests three major cellular functions of Mtm mediated by Rab11: F-actin dynamics, membrane protein distribution, and actomyosin activity. While our results suggest that actomyosin functions as the most downstream effector of Mtm in growth control, we were surprised to see that increased F-actin accumulation is not critical for tissue overgrowth induced by the loss-of-*mtm*. Given that both F-actin and actomyosin are known to regulate the Hippo pathway and tissue growth, it will be important to further investigate their regulatory relationships and respective contributions to the Hippo pathway at the cellular level. In addition to F-actin accumulation, accumulations of multiple membrane proteins were found in *mtm* mutants, including Rho1, DE-Cad, Arm, and aPKC. However, our further investigation suggests that the growth control function of Mtm is unlikely mediated by the distribution of any single membrane protein we investigated, although we cannot exclude the possibility that integrated effects of multiple membrane proteins underly the molecular mechanism of Mtm function in growth control and its synergistic interactions with the Hippo pathway.

It is worth mentioning that previous studies have suggested critical roles of intracellular vesicular trafficking in activating Hippo signaling at the plasma membrane (Verghese & Moberg, 2019). Studies in mice also indicated a critical role of Rab11 in suppressing Yap activity by maintaining LATS kinase activity and YAP localization at adherens junctions (D'Agostino *et al*, 2019; Goswami *et al*, 2021). Whether Rab11 functions similarly to regulate the activity of Wts, Yki, or both downstream of Mtm would be a question to be addressed.

An unexpected finding in this study concerns the actomyosin-independent function of Mtm on Yki phosphorylation in Kc167 cells. While actomyosin has been linked to the Hippo signaling, the role of actomyosin on Yki/YAP phosphorylation remains unclear. In certain mammalian cell culture conditions, suppressing actomyosin activity has a minor effect on YAP phosphorylation, a quite distinct observation from LatB or Cyto D treatment where YAP phosphorylation is elevated significantly (Zhao *et al*, 2012). Therefore, the observed inhibition of LatB-induced Yki phosphorylation by Mtm RNAi in Kc167 cells could be a cell-type-specific effect that is actomyosin independent. Alternatively, Mtm/Actomyosin-mediated tissue growth, specifically interommatidial cell number, may not necessarily correlate with Yki phosphorylation. The actomyosin-independent function of Mtm in Yki phosphorylation/activity and the *in vivo* role of Yki/Sd transcriptional machinery in Mtm/Actomyosin-mediated growth need further investigation.

Mutations in MTMR2, the human homolog of *Drosophila* Mtm, cause autosomal recessive CMT4B1 disease, a disorder resulting from defects of myelination in the peripheral nervous system (Bolino *et al*, 2000, 2004). The underlying molecular mechanisms remain unclear. Our work suggests that defects of endocytic trafficking and actomyosin activation contribute to the pathogenesis of the CMT4B1 disease. This finding is supported by a previous report showing that in mammals, the actin cytoskeletal regulator neural Wiskott–Aldrich syndrome protein (N-WASp) is critical for Schwann cell maturation and peripheral nerve myelination(Jin *et al*, 2011). More recent work in mice connected aberrant myelin synthesis to actomyosin function dysregulation in CMT4B1 neuropathy (Guerrero-Valero *et al*, 2021), further supporting our conclusion. Both NF2 and YAP/TAZ are involved in peripheral nerve myelination (Giovannini *et al*, 2000; Guo *et al*, 2012; Grove *et al*, 2017). However, a connection between Hippo signaling dysregulation and peripheral demyelinating disorders has not been established. By identifying Mtm/MTMR2-mediated membrane lipid PI(3)P dynamics as a novel upstream regulation of actomyosin and linking Mtm/MTMR2 to Hippo signaling, our work sheds novel insights into the mechanistic basis of peripheral nerve myelination and related human disorders.

Materials and Methods

Drosophila genetics

Wild-type male flies were treated with EMS overnight to induce random genomic mutation. *40A-B89* was identified as a lethal growth-regulatory candidate. *UAS-GFP-myc-2xFYVE* (mobilized to the third chromosome by Δ2-3 mobilization), *UAS-2xOsh2PH-GFP*, and *UAS-PLCδ-PH-EGFP* were recombined with *Tub-Gal4* for further analysis with mtm^{null} mutant. Fly stocks obtained from the Bloomington *Drosophila* Stock Center include the following: *UAS-pi3k68dRNAi* (stock IDs 35265, 34621, 31252), *UAS-vps34RNAi* (stock IDs 33384 and 36056), *UAS-sqh-mCherry* (stock ID 59024), *UAS-rokRNAi* (stock ID 34324), *UAS-sqhRNAi* (stock ID 33891), $UAS\text{-}rab5^{S43N}$ (stock ID 9772), $UAS\text{-}rab5^{Q88L}$ (stock ID 9773), $UAS\text{-}rab7^{T22N}$ (stock ID 9778), $UAS\text{-}rab7^{Q67L}$ (stock ID 9779), $UAS\text{-}rab11^{S25N}$ (stock ID 23261), $UAS\text{-}rab11^{Q70L}$ (stock ID 9791), *UAS-GFP-myc-2xFYVE* (stock ID 42712), *UAS-2xOsh2PH-GFP* (stock ID 57353), *UAS-PLCδ-PH-GFP* (stock ID 39693), *Tub-Gal4* (stock ID 5138), *UAS-fab1RNAi* (stock ID 35793), $vps34^{\Delta m22}$ (a gift from Gabor Juhasz), *UAS-sktlRNAi* (stock ID 27715), *UAS-PI4KIIIαRNAi* (stock ID 35256), *UAS-arpc1RNAi* (stock ID 31246), ex^{e1}, ft^{8}, mer^{4}, $kibra^{\Delta}$, $crb^{82\text{-}04}$, $hpo^{42\text{-}48}$, $pten^{129}$ (gifts from Duojia Pan), *UAS-rho1RNAi* (stock ID 9910), *UAS-shgRNAi* (stock ID 32904), *UAS-armRNAi* (stock ID 35004), *UAS-αPKCRNAi* (stock ID 34332). All crosses were performed at 25°C.

Generation of mtm mutant alleles

The method was adapted from a previous report (Ren *et al*, 2013). Briefly, two *mtm* targeting sgRNAs were designed at DRSC/Trip Functional Genomics Resources (https://www.flyrnai.org/crispr/index.html). The sgRNA 1 targeting sequence was 5′-CCGTAC CGCGGCCCCGTCTT-3′, and the sgRNA 2 targeting sequence was 5′-AGTATAGGCCCTTCCACAAG-3′. The two sgRNAs were cloned into the U6b-sgRNA-short vector, verified by sequencing and then injected into the transgenic Cas9 fly (stock ID 54591). The parent F0 adult files were used for propagation of progeny, and the primary screening was performed at the F1 progeny using the screening primers below: F1, 5′-TTGCGTGAGTTGGCAGC-3′; F2, 5′-GCGAC CAAGCTAAACGAG-3′; R, 5′-CTGAGCTGCGAAAACGC-3′.

Genotypes used for generating mutant clones or MARCM clones are shown below

mtm, *mer*, *ex*, *ft*, *kibra*, and *Crb* clones generated with eyFlp or hsFlp

eyFlp/+; FRT40A GFP/FRT40A mtm^{B89}

eyFlp/+; FRT40A GFP/FRT40A mtm^{null}

eyFlp/+; FRT40A GFP/FRT40A $mtm^{\Delta N}$

eyFlp/+; FRT40A GFP/FRT40A $mtm^{\Delta C}$

hsFlp/+; FRT40A GFP/FRT40A mtm^{null}

eyFlp FRT19A GFP/ FRT19A mer^4

eyFlp/+; FRT40A GFP/FRT40A ex^{e1}

eyFlp/+; FRT40A GFP/FRT40A ft^8

eyFlp/+; FRT82B GFP/ FRT82B $kibra^{del}$

eyFlp/+; FRT82B GFP/ FRT82B Crb^{del}

mer;mtm, *ex,mtm*, *ft,mtm*, *mtm;kibra* double mutant clones

FRT19A mer^4/Y; FRT40A GFP [mer+]/FRT40A mtm^{null}; eyFlp/+

FRT19A mer^4/Y; FRT40A GFP [mer^+]/FRT40A $mtm^{\Delta N}$; eyFlp/+

FRT19A mer^4/Y; FRT40A GFP [mer^+]/FRT40A $mtm^{\Delta C}$; eyFlp/+

eyFlp/+; FRT40A GFP/FRT40A ex^{e1},$mtm^{\Delta N}$

eyFlp/+; FRT40A GFP/FRT40A ex^{e1},$mtm^{\Delta C}$

eyFlp/+; FRT40A GFP/FRT40A ex^{e1},mtm^{null}

eyFlp/+; FRT40A GFP/FRT40A ft^8,mtm^{null}

eyFlp/+; FRT40A GFP/FRT40A mtm^{null}; FRT82B RFP/ FRT82B $kibra^{del}$

eyFlp/+; FRT40A GFP/FRT40A mtm^{null}; FRT82B RFP/ FRT82B Crb^{del}

mtm clones with PI(3)P, PI(4)P, PI(4,5)P_2 reporters

hsFlp/+; FRT40A RFP/FRT40A mtm^{null}; Tub-Gal4, UAS-GFP-myc-2xFYVE/+

hsFlp/+; FRT40A RFP/FRT40A mtm^{null}; Tub-Gal4, UAS-2xOsh2PH-GFP/+

hsFlp/+; FRT40A RFP/FRT40A mtm^{null}; Tub-Gal4, UAS-PLCδ-PH-EGFP/+

MARCM clones overexpressing *pi3k68dRNAi*, *rokRNAi*, *sqhRNAi*, *arpc1RNAi*, *rab11*, and *MTMR2*

UAS-GFP, hsflp; FRT40, Tub-Gal80/FRT40A; Tub-Gal4/UAS-pi3k68dRNAi

UAS-GFP, hsflp; FRT40, Tub-Gal80/FRT40A; Tub-Gal4/UAS-rokRNAi

UAS-GFP, hsflp; FRT40, Tub-Gal80/FRT40A; Tub-Gal4/UAS-sqhRNAi

UAS-GFP, hsflp; FRT40, Tub-Gal80/FRT40A; Tub-Gal4/UAS-arpc1RNAi

UAS-GFP, hsflp; FRT40, Tub-Gal80/FRT40A; Tub-Gal4/UAS-$rab11^{Q70L}$

UAS-GFP, hsflp; FRT40, Tub-Gal80/FRT40A; Tub-Gal4/UAS-MTMR2

Flip-out clones overexpressing $rab11^{S25N}$

hsFlp/+; Act>CD2>Gal4, UAS-GFP/+; UAS-$rab11^{S25N}$/+

mtm, *mer*, *ex*, *ft*, *hpo*, *ex,mtm*, *ft,mtm* MARCM clones with or without overexpressing *pi3k68dRNAi*, *sqh-mCherry*, *rho1RNAi*, *rokRNAi*, *sqhRNAi*, *vps34RNAi*, *fab1RNAi*, *sktlRNAi*, *PI4KIIIαRNAi*, *arpc1RNAi*, *shgRNAi*, *armRNAi*, *αPKCRNAi*, *rab5*, *rab7*, *rab11* and *MTMR2*

UAS-GFP, hsflp; FRT40, Tub-Gal80/FRT40A mtm^{null}; Tub-Gal4/+

UAS-GFP, hsflp; FRT40, Tub-Gal80/FRT40A mtm^{null}; Tub-Gal4/UAS-pi3k68dRNAi

UAS-GFP, hsflp; FRT40, Tub-Gal80/FRT40A mtm^{null}; Tub-Gal4/UAS-vps34RNAi

UAS-GFP, hsflp; FRT40, Tub-Gal80/FRT40A mtm^{null}; Tub-Gal4/UAS-fab1RNAi

UAS-GFP, hsflp; FRT40, Tub-Gal80/FRT40A mtm^{null}; Tub-Gal4/UAS-sktlRNAi

UAS-GFP, hsflp; FRT40, Tub-Gal80/FRT40A mtm^{null}; Tub-Gal4/UAS-PI4KIIIαRNAi

UAS-GFP, hsflp; FRT40, Tub-Gal80/FRT40A mtm^{null}; Tub-Gal4/UAS-sqh-mCherry

UAS-GFP, hsflp; FRT40, Tub-Gal80/FRT40A ex^{e1},mtm^{null}; Tub-Gal4/+

UAS-GFP, hsflp; FRT40, Tub-Gal80/FRT40A ft^8,mtm^{null}; Tub-Gal4/+

UAS-GFP, hsflp; FRT40, Tub-Gal80/FRT40A ex^{e1},mtm^{null}; Tub-Gal4/UAS-pi3k68dRNAi

UAS-GFP, hsflp; FRT40, Tub-Gal80/FRT40A ft^8,mtm^{null}; Tub-Gal4/UAS-pi3k68dRNAi

UAS-GFP, hsflp; FRT40, Tub-Gal80/FRT40A mtm^{null}; Tub-Gal4/UAS-arpc1RNAi

UAS-GFP, hsflp; FRT40, Tub-Gal80/FRT40A mtm^{null}; Tub-Gal4/UAS-rho1RNAi

UAS-GFP, hsflp; FRT40, Tub-Gal80/FRT40A mtm^{null}; Tub-Gal4/UAS-rokRNAi

UAS-GFP, hsflp; FRT40, Tub-Gal80/FRT40A mtm^{null}; Tub-Gal4/UAS-sqhRNAi

UAS-GFP, hsflp; FRT40, Tub-Gal80/FRT40A ex^{e1},mtm^{null}; Tub-Gal4/UAS-rokRNAi

UAS-GFP, hsflp; FRT40, Tub-Gal80/FRT40A ft^8,mtm^{null}; Tub-Gal4/UAS-rokRNAi

UAS-GFP, hsflp; FRT40, Tub-Gal80/FRT40A mtm^{null}; Tub-Gal4/UAS-$rab5^{S43N}$

UAS-GFP, hsflp; FRT40, Tub-Gal80/FRT40A mtm^{null}; Tub-Gal4/UAS-$rab5^{Q88L}$

UAS-GFP, hsflp; FRT40, Tub-Gal80/FRT40A mtm^{null}; Tub-Gal4/UAS-$rab7^{T22N}$

UAS-GFP, hsflp; FRT40, Tub-Gal80/FRT40A mtm^{null}; Tub-Gal4/UAS-$rab7^{Q67L}$

UAS-GFP, hsflp; FRT40, Tub-Gal80/FRT40A mtm^{null}; Tub-Gal4/UAS-$rab11^{S25N}$

UAS-GFP, hsflp; FRT40, Tub-Gal80/FRT40A mtm^{null}; Tub-Gal4/UAS-$rab11^{Q70L}$

UAS-GFP, hsflp; FRT40, Tub-Gal80/FRT40A ex^{e1},mtm^{null}; Tub-Gal4/UAS-$rab11^{Q70L}$

UAS-GFP, hsflp; FRT40, Tub-Gal80/FRT40A ft^8,mtm^{null}; Tub-Gal4/UAS-$rab11^{Q70L}$

UAS-GFP, hsflp; FRT40, Tub-Gal80/FRT40A mtm^{null}; Tub-Gal4/UAS-shgRNAi

UAS-GFP, hsflp; FRT40, Tub-Gal80/FRT40A mtm^{null}; Tub-Gal4/UAS-armRNAi

UAS-GFP, hsflp; FRT40, Tub-Gal80/FRT40A mtm^{null}; Tub-Gal4/UAS-αPKCRNAi

UAS-GFP, hsflp; FRT40, Tub-Gal80/FRT40A mtm^{null}; Tub-Gal4/UAS-MTMR2

UAS-GFP, hsflp; FRT40, Tub-Gal80/FRT40A mtm^{null}; Tub-Gal4/UAS-$MTMR2^{G103E}$

UAS-GFP, hsflp; FRT40, Tub-Gal80/FRT40A ex^{e1},mtm^{null}; Tub-Gal4/UAS-MTMR2

UAS-GFP, hsflp; FRT40, Tub-Gal80/FRT40A ex^{e1}; Tub-Gal4/UAS-UAS-pi3k68dRNAi

UAS-GFP, hsflp; FRT40, Tub-Gal80/FRT40A ft^{8}; Tub-Gal4/UAS-UAS-pi3k68dRNAi

UAS-GFP, hsflp; FRT40, Tub-Gal80/FRT40A ex^{e1}; Tub-Gal4/UAS-rokRNAi

UAS-GFP, hsflp; FRT40, Tub-Gal80/FRT40A ft^{8}; Tub-Gal4/UAS-rokRNAi

UAS-GFP, hsflp; FRT40, Tub-Gal80/FRT40A ex^{e1}; Tub-Gal4/UAS-$rab11^{Q70L}$

UAS-GFP, hsflp; FRT40, Tub-Gal80/FRT40A ft^{8}; Tub-Gal4/UAS-$rab11^{Q70L}$

Tub-Gal80, hsflp, FRT19/FRT19 mer^{4}; UAS-GFP/+; Tub-Gal4/UAS-$rab11^{S25N}$

UAS-GFP, hsflp; FRT40, Tub-Gal80/FRT40A ex^{e1}; Tub-Gal4/UAS-$rab11^{S25N}$

UAS-GFP, hsflp; FRT42, Tub-Gal80/FRT42D $hpo^{42\text{-}48}$; Tub-Gal4/+

Construction of transgenic flies

The human MTMR2 CDS sequence (GenBank: BC040432.1) was used for construction of the MTMR2 transgenic constructs. The G103E mutation was introduced into the MTMR2 CDS sequence by primer-mediated site-directed mutagenesis. Then, the MTMR2 and $MTMR2^{G103E}$ CDS sequences were cloned into the pUAST-attB vector for P-element-mediated transformation (BestGene Inc.).

Immunofluorescence

Wandering third instar larvae were dissected for eye discs and wing discs. All pupal eye discs were dissected at ~ 40 h post puparium formation. Larval eye discs, wing discs, pupal eye disc, and ovaries were fixed with 4% paraformaldehyde/PBS solution for 15 min, permeabilized, and washed in PBS containing 0.3% Triton X-100 and stained with the following primary antibodies: mouse anti-Dlg (1:50; Developmental Studies Hybridoma Bank [DHSB]), mouse anti-Diap1 (1:500; DHSB), mouse anti-rab7 (1:100; DHSB), rat anti-DE-Cadherin (1:25; DHSB), rat anti-Armadillo (1:50; DHSB), guinea pig anti-Ex (1:2,000, a gift from Richard Fehon), guinea pig anti-Mer (1:2,000, a gift from Richard Fehon), rabbit anti-Yki (1:1,000, a gift from Duojia Pan), rabbit anti-p-MLC (1:10; Cell Signaling Technologies), rabbit anti-rab5 (1:1,000; Abcam), mouse anti-Rab11 (1:20; BD Biosciences), rabbit anti-rab11 (1:750; a gift from Donald F. Ready; Satoh *et al*, 2005), mouse anti-crumbs (1:5; DHSB), and rabbit anti-Kibra (1:1,000, a gift from Duojia Pan). All secondary antibodies (Jackson ImmunoResearch Laboratory) were diluted at 1:300. For visualization of F-actin, the fixed samples were incubated with Alexa Fluor 555 phalloidin (1:500, Invitrogen) in PBS for 2 h at room temperature. For treatment with wortmannin, the dissected tissues were incubated with 100 nM wortmannin (Cayman Chemical) for 45 min at RT. For analysis of the transferrin endocytosis and trafficking, the dissected ovaries were incubated with 25 μg/ml of transferrin (Invitrogen) diluted in Schneider's *Drosophila* Medium (Gibco) for 30 min at RT. All samples were imaged using either a Carl Zeiss LSM880 or a Leica SP8 confocal microscope and analyzed using *ImageJ*.

Drosophila cell culture

Drosophila kc167 cells were purchased from DGRC and cultured in CCM3 medium (HyClone™) at 25°C. For RNAi knockdown, 5 μg of dsRNAs targeting *mtm* or *gfp* was used. To test the effects of latrunculin B on phosphorylation of Yki, the cells were treated with 50 μM latrunculin B for half an hour in complete medium before lysis of the cells.

Lipid phosphatase activity assay

The *Drosophila mtm* CDS sequence (NCBI reference sequence: NM_078765.4) was used to amplify the $mtm^{\Delta C}$ mutant CDS using the fusion primer (5′-AGCGTGAGATCGGTCCGCCTATACTGTCGCT GGAATC-3′). Both the wild-type *mtm* and $mtm^{\Delta C}$ CDSs were then cloned into the pAc5.1/V5-His B vector (Invitrogen) for transient expression of the V5-tagged Mtm proteins. Kc167 cells were seeded in 6-well plates and transfected with *V5-mtm* or *V5-*$mtm^{\Delta C}$. The empty vector transfection was used as a control. 72 h after the transfection, the cells were lysed with lysis buffer (25 mM Tris–HCl (pH 7.5), 1 mM EDTA, 1 mM EGTA, 5 mM $MgCl_2$, 150 mM NaCl, 10% glycerol, 1% NP-40, 1 mM DTT, and 1× protease inhibitor (Sigma)). Lysates were spun at 15,000 rpm for 15 min at 4°C and the supernatants were collected for co-immunoprecipitation using anti-V5 antibody (Invitrogen) and protein G agarose beads (Bio-Rad) for overnight at 4°C. The beads were collected and washed three times with the reaction buffer (25 mM Tris–HCl (pH 7.4), 140 mM NaCl, 2.7 mM KCl). A small portion of the beads was used for Western blotting and the remaining bulk was used for the PI(3)P phosphatase activity assay following the manufacturer's instructions (Echelon Biosciences, Inc.). The synthetic PI(3)P (Echelon Biosciences, Inc., #P-3008) was used as the substrate. The free phosphate in solution was measured by plate reader at 620 nm.

Fluorescence intensity quantification

Immunofluorescence images were quantified by analyzing the mean fluorescence intensity of 10 different *mtm* mutant clones and surrounding wild-type tissues in the third instar larval wing discs and eye discs from several randomly chosen confocal images using ImageJ (v1.53r, NIH).

Statistical analysis

All statistics were analyzed using Student's *t*-test with GraphPad Prism 7.0 software. Data are presented as mean ± SEM, and statistical significance is indicated as $***P < 0.001$, $****P < 0.0001$.

Data availability

This study includes no data deposited in external repositories.

Expanded View for this article is available online.

Acknowledgments

We thank Richard Fehon, Gabor Juhasz, Duojia Pan, Donald Ready, and Robert Ward for kindly providing us with reagents and fly stocks. We thank Hua Deng, Samantha Simonovitch, and Yonggang Zheng for helpful discussions and critical reading of this manuscript. We thank Bloomington Stock Center for fly stocks and the Developmental Studies Hybridoma Bank for antibodies. We thank the Confocal Microscopy Core at Kansas State University and the Advanced Microscopy Facility at the University of Connecticut. This work was supported in part by grants from the National Institutes of Health (GM136904 to J. Yu), the National Science Foundation (2115690 to J. Yu), and a start-up

fund from the University of Connecticut. Y.X. was supported by NIH/NINDS R01 NS112506, NIH/NIA K01 AG046366 award, Parkinson's Foundation Stanley Fahn Junior Faculty award PF-JFA-1934, American Parkinson Disease Association (APDA) research grant.

Author contributions

Liang Hu: Conceptualization; formal analysis; validation; investigation; writing – original draft; writing – review and editing. **Wyatt Brichalli:** Validation; investigation; writing – review and editing. **Naren Li:** Validation; investigation; writing – review and editing. **Shifan Chen:** Validation; investigation; writing – review and editing. **Yaqing Cheng:** Validation; investigation; writing – review and editing. **Qinfang Liu:** Validation; investigation; writing – review and editing. **Yulan Xiong:** Conceptualization; resources; supervision; funding acquisition; validation; project administration; writing – review and editing. **Jianzhong Yu:** Conceptualization; resources; formal analysis; supervision; funding acquisition; validation; investigation; writing – original draft; project administration; writing – review and editing.

Disclosure and competing interests statement

The authors declare that they have no competing interests.

References

Aragona M, Panciera T, Manfrin A, Giulitti S, Michielin F, Elvassore N, Dupont S, Piccolo S (2013) A mechanical checkpoint controls multicellular growth through YAP/TAZ regulation by actin-processing factors. *Cell* 154: 1047 – 1059

Balla T (2013) Phosphoinositides: tiny lipids with giant impact on cell regulation. *Physiol Rev* 93: 1019 – 1137

Begley MJ, Taylor GS, Kim SA, Veine DM, Dixon JE, Stuckey JA (2003) Crystal structure of a phosphoinositide phosphatase, MTMR2: insights into myotubular myopathy and Charcot-Marie-Tooth syndrome. *Mol Cell* 12: 1391 – 1402

Berger P, Bonneick S, Willi S, Wymann M, Suter U (2002) Loss of phosphatase activity in myotubularin-related protein 2 is associated with Charcot-Marie-Tooth disease type 4B1. *Hum Mol Genet* 11: 1569 – 1579

Boggiano JC, Fehon RG (2012) Growth control by committee: intercellular junctions, cell polarity, and the cytoskeleton regulate Hippo signaling. *Dev Cell* 22: 695 – 702

Bolino A, Brancolini V, Bono F, Bruni A, Gambardella A, Romeo G, Quattrone A, Devoto M (1996) Localization of a gene responsible for autosomal recessive demyelinating neuropathy with focally folded myelin sheaths to chromosome 11q23 by homozygosity mapping and haplotype sharing. *Hum Mol Genet* 5: 1051 – 1054

Bolino A, Muglia M, Conforti FL, LeGuern E, Salih MA, Georgiou DM, Christodoulou K, Hausmanowa-Petrusewicz I, Mandich P, Schenone A *et al* (2000) Charcot-Marie-Tooth type 4B is caused by mutations in the gene encoding myotubularin-related protein-2. *Nat Genet* 25: 17 – 19

Bolino A, Bolis A, Previtali SC, Dina G, Bussini S, Dati G, Amadio S, Del Carro U, Mruk DD, Feltri ML *et al* (2004) Disruption of Mtmr2 produces CMT4B1-like neuropathy with myelin outfolding and impaired spermatogenesis. *J Cell Biol* 167: 711 – 721

Bonneick S, Boentert M, Berger P, Atanasoski S, Mantei N, Wessig C, Toyka KV, Young P, Suter U (2005) An animal model for Charcot-Marie-Tooth disease type 4B1. *Hum Mol Genet* 14: 3685 – 3695

Cagan RL, Ready DF (1989) The emergence of order in the *Drosophila* pupal retina. *Dev Biol* 136: 346 – 362

Calses PC, Crawford JJ, Lill JR, Dey A (2019) Hippo pathway in cancer: aberrant regulation and therapeutic opportunities. *Trends Cancer* 5: 297 – 307

Campa CC, Hirsch E (2017) Rab11 and phosphoinositides: a synergy of signal transducers in the control of vesicular trafficking. *Adv Biol Regul* 63: 132 – 139

Campa CC, Margaria JP, Derle A, Del Giudice M, De Santis MC, Gozzelino L, Copperi F, Bosia C, Hirsch E (2018) Rab11 activity and PtdIns(3)P turnover removes recycling cargo from endosomes. *Nat Chem Biol* 14: 801 – 810

Chinthalapudi K, Mandati V, Zheng J, Sharff AJ, Bricogne G, Griffin PR, Kissil J, Izard T (2018) Lipid binding promotes the open conformation and tumor-suppressive activity of neurofibromin 2. *Nat Commun* 9: 1338

Choi KW (2018) Upstream paths for Hippo signaling in *Drosophila* organ development. *BMB Rep* 51: 134 – 142

D'Agostino L, Nie Y, Goswami S, Tong K, Yu S, Bandyopadhyay S, Flores J, Zhang X, Balasubramanian I, Joseph I *et al* (2019) Recycling endosomes in mature epithelia restrain tumorigenic signaling. *Cancer Res* 79: 4099 – 4112

Deng H, Wang W, Yu J, Zheng Y, Qing Y, Pan D (2015) Spectrin regulates Hippo signaling by modulating cortical actomyosin activity. *Elife* 4: e06567

Deng H, Yang L, Wen P, Lei H, Blount P, Pan D (2020) Spectrin couples cell shape, cortical tension, and Hippo signaling in retinal epithelial morphogenesis. *J Cell Biol* 219: e201907018

Dupont S, Morsut L, Aragona M, Enzo E, Giulitti S, Cordenonsi M, Zanconato F, Le Digabel J, Forcato M, Bicciato S *et al* (2011) Role of YAP/TAZ in mechanotransduction. *Nature* 474: 179 – 183

Fernandez BG, Gaspar P, Bras-Pereira C, Jezowska B, Rebelo SR, Janody F (2011) Actin-capping protein and the Hippo pathway regulate F-actin and tissue growth in *Drosophila*. *Development* 138: 2337 – 2346

Fletcher GC, Elbediwy A, Khanal I, Ribeiro PS, Tapon N, Thompson BJ (2015) The Spectrin cytoskeleton regulates the Hippo signalling pathway. *EMBO J* 34: 940 – 954

Franco I, Gulluni F, Campa CC, Costa C, Margaria JP, Ciraolo E, Martini M, Monteyne D, De Luca E, Germena G *et al* (2014) PI3K class II alpha controls spatially restricted endosomal PtdIns3P and Rab11 activation to promote primary cilium function. *Dev Cell* 28: 647 – 658

Fulford A, Tapon N, Ribeiro PS (2018) Upstairs, downstairs: spatial regulation of Hippo signalling. *Curr Opin Cell Biol* 51: 22 – 32

Gaspar P, Tapon N (2014) Sensing the local environment: actin architecture and Hippo signalling. *Curr Opin Cell Biol* 31: 74 – 83

Genevet A, Polesello C, Blight K, Robertson F, Collinson LM, Pichaud F, Tapon N (2009) The Hippo pathway regulates apical-domain size independently of its growth-control function. *J Cell Sci* 122: 2360 – 2370

Gillooly DJ, Morrow IC, Lindsay M, Gould R, Bryant NJ, Gaullier JM, Parton RG, Stenmark H (2000) Localization of phosphatidylinositol 3-phosphate in yeast and mammalian cells. *EMBO J* 19: 4577 – 4588

Giovannini M, Robanus-Maandag E, van der Valk M, Niwa-Kawakita M, Abramowski V, Goutebroze L, Woodruff JM, Berns A, Thomas G (2000) Conditional biallelic Nf2 mutation in the mouse promotes manifestations of human neurofibromatosis type 2. *Genes Dev* 14: 1617 – 1630

Goswami S, Balasubramanian I, D'Agostino L, Bandyopadhyay S, Patel R, Avasthi S, Yu S, Goldenring JR, Bonder EM, Gao N (2021) RAB11A-mediated YAP localization to adherens and tight junctions is essential for colonic epithelial integrity. *J Biol Chem* 297: 100848

Grove M, Kim H, Santerre M, Krupka AJ, Han SB, Zhai J, Cho JY, Park R, Harris M, Kim S *et al* (2017) YAP/TAZ initiate and maintain Schwann cell myelination. *eLife* 6: e20982

Grusche FA, Richardson HE, Harvey KF (2010) Upstream regulation of the hippo size control pathway. *Curr Biol* 20: R574 – R582

Grzeschik NA, Parsons LM, Allott ML, Harvey KF, Richardson HE (2010) Lgl, aPKC, and Crumbs regulate the Salvador/Warts/Hippo pathway through two distinct mechanisms. *Curr Biol* 20: 573 – 581

Guerrero-Valero M, Grandi F, Cipriani S, Alberizzi V, Di Guardo R, Chicanne G, Sawade L, Bianchi F, Del Carro U, De Curtis I *et al* (2021) Dysregulation of myelin synthesis and actomyosin function underlies aberrant myelin in CMT4B1 neuropathy. *Proc Natl Acad Sci U S A* 118: e2009469118

Guo L, Moon C, Niehaus K, Zheng Y, Ratner N (2012) Rac1 controls Schwann cell myelination through cAMP and NF2/merlin. *J Neurosci* 32: 17251 – 17261

Halder G, Johnson RL (2011) Hippo signaling: growth control and beyond. *Development* 138: 9 – 22

Hamaratoglu F, Willecke M, Kango-Singh M, Nolo R, Hyun E, Tao C, Jafar-Nejad H, Halder G (2006) The tumour-suppressor genes NF2/Merlin and Expanded act through Hippo signalling to regulate cell proliferation and apoptosis. *Nat Cell Biol* 8: 27 – 36

Hamaratoglu F, Gajewski K, Sansores-Garcia L, Morrison C, Tao C, Halder G (2009) The Hippo tumor-suppressor pathway regulates apical-domain size in parallel to tissue growth. *J Cell Sci* 122: 2351 – 2359

Han Y (2019) Analysis of the role of the Hippo pathway in cancer. *J Transl Med* 17: 116

Han H, Qi R, Zhou JJ, Ta AP, Yang B, Nakaoka HJ, Seo G, Guan KL, Luo R, Wang W (2018) Regulation of the hippo pathway by phosphatidic acid-mediated lipid-protein interaction. *Mol Cell* 72: 328 – 340.e8

Harvey KF, Hariharan IK (2012) The hippo pathway. *Cold Spring Harb Perspect Biol* 4: a011288

Hong AW, Meng Z, Plouffe SW, Lin Z, Zhang M, Guan KL (2020) Critical roles of phosphoinositides and NF2 in Hippo pathway regulation. *Genes Dev* 34: 511 – 525

Houlden H, King RH, Wood NW, Thomas PK, Reilly MM (2001) Mutations in the 5′ region of the myotubularin-related protein 2 (MTMR2) gene in autosomal recessive hereditary neuropathy with focally folded myelin. *Brain* 124: 907 – 915

Jean S, Cox S, Schmidt EJ, Robinson FL, Kiger A (2012) Sbf/MTMR13 coordinates PI(3)P and Rab21 regulation in endocytic control of cellular remodeling. *Mol Biol Cell* 23: 2723 – 2740

Jin F, Dong B, Georgiou J, Jiang Q, Zhang J, Bharioke A, Qiu F, Lommel S, Feltri ML, Wrabetz L *et al* (2011) N-WASp is required for Schwann cell cytoskeletal dynamics, normal myelin gene expression and peripheral nerve myelination. *Development* 138: 1329 – 1337

Ketel K, Krauss M, Nicot AS, Puchkov D, Wieffer M, Muller R, Subramanian D, Schultz C, Laporte J, Haucke V (2016) A phosphoinositide conversion mechanism for exit from endosomes. *Nature* 529: 408 – 412

Kim W, Jho EH (2018) The history and regulatory mechanism of the hippo pathway. *BMB Rep* 51: 106 – 118

Lindmo K, Stenmark H (2006) Regulation of membrane traffic by phosphoinositide 3-kinases. *J Cell Sci* 119: 605 – 614

Ling C, Zheng Y, Yin F, Yu J, Huang J, Hong Y, Wu S, Pan D (2010) The apical transmembrane protein crumbs functions as a tumor suppressor that regulates Hippo signaling by binding to Expanded. *Proc Natl Acad Sci U S A* 107: 10532 – 10537

Lorenzo O, Urbe S, Clague MJ (2006) Systematic analysis of myotubularins: heteromeric interactions, subcellular localisation and endosome related functions. *J Cell Sci* 119: 2953 – 2959

Ma S, Meng Z, Chen R, Guan KL (2019) The Hippo pathway: biology and pathophysiology. *Annu Rev Biochem* 88: 577 – 604

Maitra S, Kulikauskas RM, Gavilan H, Fehon RG (2006) The tumor suppressors merlin and expanded function cooperatively to modulate receptor endocytosis and signaling. *Curr Biol* 16: 702 – 709

Marat AL, Haucke V (2016) Phosphatidylinositol 3-phosphates-at the interface between cell signalling and membrane traffic. *EMBO J* 35: 561 – 579

Matsui Y, Lai ZC (2013) Mutual regulation between Hippo signaling and actin cytoskeleton. *Protein Cell* 4: 904 – 910

Meng Z, Moroishi T, Guan KL (2016) Mechanisms of Hippo pathway regulation. *Genes Dev* 30: 1 – 17

Misra JR, Irvine KD (2018) The Hippo signaling network and its biological functions. *Annu Rev Genet* 52: 65 – 87

Morel E, Chamoun Z, Lasiecka ZM, Chan RB, Williamson RL, Vetanovetz C, Dall'Armi C, Simoes S, Point Du Jour KS, McCabe BD *et al* (2013) Phosphatidylinositol-3-phosphate regulates sorting and processing of amyloid precursor protein through the endosomal system. *Nat Commun* 4: 2250

Nielsen E, Christoforidis S, Uttenweiler-Joseph S, Miaczynska M, Dewitte F, Wilm M, Hoflack B, Zerial M (2000) Rabenosyn-5, a novel Rab5 effector, is complexed with hVPS45 and recruited to endosomes through a FYVE finger domain. *J Cell Biol* 151: 601 – 612

Pan D (2007) Hippo signaling in organ size control. *Genes Dev* 21: 886 – 897

Pan D (2010) The Hippo signaling pathway in development and cancer. *Dev Cell* 19: 491 – 505

Previtali SC, Quattrini A, Bolino A (2007) Charcot-Marie-Tooth type 4B demyelinating neuropathy: deciphering the role of MTMR phosphatases. *Expert Rev Mol Med* 9: 1 – 16

Rausch V, Hansen CG (2020) The hippo pathway, YAP/TAZ, and the plasma membrane. *Trends Cell Biol* 30: 32 – 48

Rauskolb C, Sun S, Sun G, Pan Y, Irvine KD (2014) Cytoskeletal tension inhibits Hippo signaling through an Ajuba-Warts complex. *Cell* 158: 143 – 156

Ren X, Sun J, Housden BE, Hu Y, Roesel C, Lin S, Liu LP, Yang Z, Mao D, Sun L *et al* (2013) Optimized gene editing technology for *Drosophila* melanogaster using germ line-specific Cas9. *Proc Natl Acad Sci U S A* 110: 19012 – 19017

Robinson FL, Dixon JE (2006) Myotubularin phosphatases: policing 3-phosphoinositides. *Trends Cell Biol* 16: 403 – 412

Sansores-Garcia L, Bossuyt W, Wada K, Yonemura S, Tao C, Sasaki H, Halder G (2011) Modulating F-actin organization induces organ growth by affecting the Hippo pathway. *EMBO J* 30: 2325 – 2335

Satoh AK, O'Tousa JE, Ozaki K, Ready DF (2005) Rab11 mediates post-Golgi trafficking of rhodopsin to the photosensitive apical membrane of *Drosophila* photoreceptors. *Development* 132: 1487 – 1497

Seo J, Kim J (2018) Regulation of Hippo signaling by actin remodeling. *BMB Rep* 51: 151 – 156

Simonsen A, Lippe R, Christoforidis S, Gaullier JM, Brech A, Callaghan J, Toh BH, Murphy C, Zerial M, Stenmark H (1998) EEA1 links PI(3)K function to Rab5 regulation of endosome fusion. *Nature* 394: 494 – 498

Singla A, Fedoseienko A, Giridharan SSP, Overlee BL, Lopez A, Jia D, Song J, Huff-Hardy K, Weisman L, Burstein E *et al* (2019) Endosomal PI(3)P regulation by the COMMD/CCDC22/CCDC93 (CCC) complex controls membrane protein recycling. *Nat Commun* 10: 4271

Steinfeld N, Lahiri V, Morrison A, Metur SP, Klionsky DJ, Weisman LS (2021) Elevating PI3P drives select downstream membrane trafficking pathways. *Mol Biol Cell* 32: 143 – 156

Stenmark H (2009) Rab GTPases as coordinators of vesicle traffic. *Nat Rev Mol Cell Biol* 10: 513 – 525

Su T, Ludwig MZ, Xu J, Fehon RG (2017) Kibra and Merlin activate the hippo pathway spatially distinct from and independent of expanded. *Dev Cell* 40: 478 – 490.e3

Sun S, Irvine KD (2016) Cellular organization and cytoskeletal regulation of the hippo signaling network. *Trends Cell Biol* 26: 694 – 704

Tapon N, Harvey KF (2012) The Hippo pathway--from top to bottom and everything in between. *Semin Cell Dev Biol* 23: 768 – 769

Taylor GS, Maehama T, Dixon JE (2000) Myotubularin, a protein tyrosine phosphatase mutated in myotubular myopathy, dephosphorylates the lipid second messenger, phosphatidylinositol 3-phosphate. *Proc Natl Acad Sci U S A* 97: 8910 – 8915

Ullrich O, Reinsch S, Urbe S, Zerial M, Parton RG (1996) Rab11 regulates recycling through the pericentriolar recycling endosome. *J Cell Biol* 135: 913 – 924

Velichkova M, Juan J, Kadandale P, Jean S, Ribeiro I, Raman V, Stefan C, Kiger AA (2010) *Drosophila Mtm* and class II PI3K coregulate a PI(3)P pool with cortical and endolysosomal functions. *J Cell Biol* 190: 407 – 425

Verghese S, Moberg K (2019) Roles of membrane and vesicular traffic in regulation of the hippo pathway. *Front Cell Dev Biol* 7: 384

Vicente-Manzanares M, Ma X, Adelstein RS, Horwitz AR (2009) Non-muscle myosin II takes centre stage in cell adhesion and migration. *Nat Rev Mol Cell Biol* 10: 778 – 790

Wolff T, Ready DF (1991) Cell death in normal and rough eye mutants of *Drosophila*. *Development* 113: 825 – 839

Xu J, Vanderzalm PJ, Ludwig M, Su T, Tokamov SA, Fehon RG (2018) Yorkie functions at the cell cortex to promote myosin activation in a non-transcriptional manner. *Dev Cell* 46: 271 – 284.e5

Yan Y, Denef N, Tang C, Schupbach T (2011) *Drosophila* PI4KIIIalpha is required in follicle cells for oocyte polarization and Hippo signaling. *Development* 138: 1697 – 1703

Yin F, Yu J, Zheng Y, Chen Q, Zhang N, Pan D (2013) Spatial organization of Hippo signaling at the plasma membrane mediated by the tumor suppressor Merlin/NF2. *Cell* 154: 1342 – 1355

Yu FX, Guan KL (2013) The Hippo pathway: regulators and regulations. *Genes Dev* 27: 355 – 371

Yu J, Poulton J, Huang YC, Deng WM (2008) The hippo pathway promotes notch signaling in regulation of cell differentiation, proliferation, and oocyte polarity. *PLoS One* 3: e1761

Yu J, Zheng Y, Dong J, Klusza S, Deng WM, Pan D (2010) Kibra functions as a tumor suppressor protein that regulates Hippo signaling in conjunction with Merlin and Expanded. *Dev Cell* 18: 288 – 299

Yu FX, Zhao B, Guan KL (2015) Hippo pathway in organ size control, tissue homeostasis, and cancer. *Cell* 163: 811 – 828

Zhao B, Li L, Wang L, Wang CY, Yu J, Guan KL (2012) Cell detachment activates the Hippo pathway via cytoskeleton reorganization to induce anoikis. *Genes Dev* 26: 54 – 68

Zheng Y, Pan D (2019) The hippo signaling pathway in development and disease. *Dev Cell* 50: 264 – 282

Zoncu R, Perera RM, Balkin DM, Pirruccello M, Toomre D, De Camilli P (2009) A phosphoinositide switch controls the maturation and signaling properties of APPL endosomes. *Cell* 136: 1110 – 1121